AUG 8 2000

SANDIA REPORT

SAND2000-1767
Unlimited Release
Printed July 2000

Radiation of Elastic Waves from Point Sources in a Uniform Wholespace

David F. Aldridge

RECEIVED
AUG 22 2000
OSTI

Prepared by
Sandia National Laboratories
Albuquerque, New Mexico 87185 and Livermore, California 94550

Sandia is a multiprogram laboratory operated by Sandia Corporation, a Lockheed Martin Company, for the United States Department of Energy under Contract DE-AC04-94AL85000.

Approved for public release; further dissemination unlimited.

Sandia National Laboratories

Issued by Sandia National Laboratories, operated for the United States Department of Energy by Sandia Corporation.

NOTICE: This report was prepared as an account of work sponsored by an agency of the United States Government. Neither the United States Government, nor any agency thereof, nor any of their employees, nor any of their contractors, subcontractors, or their employees, make any warranty, express or implied, or assume any legal liability or responsibility for the accuracy, completeness, or usefulness of any information, apparatus, product, or process disclosed, or represent that its use would not infringe privately owned rights. Reference herein to any specific commercial product, process, or service by trade name, trademark, manufacturer, or otherwise, does not necessarily constitute or imply its endorsement, recommendation, or favoring by the United States Government, any agency thereof, or any of their contractors or subcontractors. The views and opinions expressed herein do not necessarily state or reflect those of the United States Government, any agency thereof, or any of their contractors.

Printed in the United States of America. This report has been reproduced directly from the best available copy.

Available to DOE and DOE contractors from
U.S. Department of Energy
Office of Scientific and Technical Information
P.O. Box 62
Oak Ridge, TN 37831

Telephone: (865)576-8401
Facsimile: (865)576-5728
E-Mail: reports@adonis.osti.gov
Online ordering: http://www.doe.gov/bridge

Available to the public from
U.S. Department of Commerce
National Technical Information Service
5285 Port Royal Rd
Springfield, VA 22161

Telephone: (800)553-6847
Facsimile: (703)605-6900
E-Mail: orders@ntis.fedworld.gov
Online order: http://www.ntis.gov/ordering.htm

DISCLAIMER

Portions of this document may be illegible in electronic image products. Images are produced from the best available original document.

SAND2000-1767
Unlimited Release
Printed July 2000

RADIATION OF ELASTIC WAVES FROM POINT SOURCES IN A UNIFORM WHOLESPACE

David F. Aldridge
Geophysical Technology Department
Sandia National Laboratories
P.O. Box 5800
Albuquerque, New Mexico, USA, 87185-0750

ABSTRACT

Seismograms generated by various simple point sources situated within a homogeneous and isotropic elastic wholespace are readily calculated from closed-form mathematical formulae. An obvious advantage of this approach is speed and accuracy in numerical modeling. Equations for particle velocity (equal to $\partial \mathbf{u}/\partial t$), acoustic pressure (proportional to div **u**), and particle rotation (equal to **curl u**), where **u** is the elastic particle displacement vector, are tabulated for a complete suite of point force and point moment sources. Pressure and rotation propagate with the P-wave speed and S-wave speed, respectively, and thus are useful for separating compressional and shear portions of the radiated elastic wavefields. All near-field, intermediate-field, and far-field terms are included in the formulae, and the expressions are valid for arbitrary source activation waveforms. The mathematical equations are expressed in a vector formalism independent of any particular coordinate reference frame. Hence, evaluation of the equations for general (i.e., fully three-dimensional) source-receiver configurations is facilitated. Synthetic seismic data calculated by this approach are quite useful for i) establishing the validity and accuracy of elastic responses computed by purely numerical (e.g., finite-difference or finite-element) algorithms, ii) evaluating various seismic data processing, analysis, and inversion schemes, and iii) assisting in the rational design of seismic energy sources and/or source arrays.

CONTENTS

1.0 INTRODUCTION

The elastic waves radiated from a point source in a homogeneous and isotropic wholespace have been described, with varying degrees of completeness and generality, by numerous investigators (e.g., Eringen and Suhubi, 1975; Aki and Richards, 1980, Ben-Menahem and Singh, 1981; White, 1983; Kennett, 1988). However, it is difficult (if not impossible) to locate a comprehensive mathematical treatment of the subject that could form the basis of a reasonably general synthetic seismogram algorithm.

In the present study, the equations characterizing the elastic wavefields produced by a variety of different point sources are assembled in a unified mathematical notation. Derivations of the formulae are not provided. All possible point force sources (represented by an orientation vector) and point moment sources (represented by an orientation tensor) are included. Arbitrary source activation waveforms are allowed. The radiated elastic waves are expressed in terms of the particle velocity and particle rotation vectors, and the acoustic pressure. Mathematical formulae describing these wavefield quantities contain all near-field, intermediate-field, and far-field terms. In the limiting case of vanishing shear wave speed, the expressions are applicable to an ideal fluid (i.e., acoustic) medium.

The resulting set of "closed-form" mathematical expressions describing the radiated elastic wavefields are amenable to rapid and accurate numerical evaluation. Synthetic seismic data calculated via this approach are useful for a variety of applications, including

1) assessing the veracity and accuracy of numerical algorithms designed to solve the governing partial differential equations of elastodynamics (e.g., finite-difference or finite-element algorithms).

2) testing inversion algorithms designed to recover seismic energy source parameters (i.e., location, waveform, magnitude, orientation vector or tensor) from recorded seismograms.

3) assisting in the rational design of seismic energy sources and/or source arrays.

A computational algorithm based on these equations is briefly described in section 6.0, and several example synthetic seismograms are displayed in section 7.0. These examples illustrate some interesting seismological phenomena. In particular, in a homogeneous and isotropic elastic medium, the acoustic pressure p propagates with the compressional (P-wave) speed α, and the particle rotation vector ω propagates with the shear (S-wave) speed β. Hence, pressure and rotation sensors are useful for separating the P-wave and S-wave portions of a seismic wavefield. Although pressure transducers (hydrophones) are commonly used in seismology, relatively little work has been conducted with rotation sensors (e.g., White, 1983, page 237). Also, the examples illustrate that the velocity and rotation wavefields are orthogonal: $(\mathbf{v} \cdot \omega) = 0$. The mathematical equations reveal that this orthogonality condition rigorously holds at all distances and directions from a point source. Finally, the examples indicate the range and diversity of seismic source situations that can be examined with this computational algorithm. In particular, elastic wavefields generated by spatially distributed arrays of non-interacting point sources, with or without beam-steering or focusing, are easily simulated.

The current algorithm calculates the elastic particle velocity vector, rather than the displacement or acceleration. This choice is motivated by a desire to compare calculated synthetic seismograms to analogous responses computed by a finite-difference algorithm that numerically solves the "velocity-stress" differential equations of elastodynamics (e.g., Graves, 1996). Also, velocity transducers (geophones) are the most commonly used seismic ground motion sensors. However, with some effort, the mathematical expressions for velocity presented here can be integrated and differentiated to obtain equations for displacement and acceleration, respectively.

2.0 POINT SOURCES OF ELASTIC WAVES

Consider a homogeneous and isotropic elastic wholespace characterized by P-wave speed α, S-wave speed β, and mass density ρ. A point source of elastic waves is located at position $\mathbf{x}_s$ with rectangular coordinates (x_s, y_s, z_s). A point receiver is located at another position $\mathbf{x}_r$ with coordinates (x_r, y_r, z_r). The vector pointing from source to receiver is

$$\mathbf{R} = \mathbf{x}_r - \mathbf{x}_s = (x_r - x_s)\mathbf{e}_x + (y_r - y_s)\mathbf{e}_y + (z_r - z_s)\mathbf{e}_z, \tag{2.1}$$

where $(\mathbf{e}_x, \mathbf{e}_y, \mathbf{e}_z)$ is an orthonormal triad of basis vectors for the rectangular coordinate system. A unit vector pointing in this same direction is

$$\mathbf{e}_R = \frac{\mathbf{R}}{\|\mathbf{R}\|} = \frac{(x_r - x_s)}{R}\mathbf{e}_x + \frac{(y_r - y_s)}{R}\mathbf{e}_y + \frac{(z_r - z_s)}{R}\mathbf{e}_z, \tag{2.2}$$

where $R^2 = (x_r - x_s)^2 + (y_r - y_s)^2 + (z_r - z_s)^2$ is the squared distance from source to receiver.

Expressions for the particle velocity vector **v**, acoustic pressure p, and particle rotation vector ω at the receiver are given below for various types of point sources located in a uniform elastic wholespace. The acoustic pressure within an elastic solid is defined to be $p = -1/3\ (\sigma_{xx} + \sigma_{yy} + \sigma_{zz})$ where the symbols σ_{ij} refer to components of the stress tensor. It is straightforward to demonstrate that this expression evaluates to $p = -K$ div **u**, where K is the bulk modulus ($K = \rho\alpha^2\ [1-(4/3)\gamma^2]$ where $\gamma \equiv \beta/\alpha$) and **u** is the particle displacement vector. Particle rotation is defined as ω = **curl u**; note that rotation is a dimensionless quantity.

Independent variables in the following equations are the source-receiver radius R, the source-to-receiver unit direction vector $\mathbf{e}_R$, and the P-wave and S-wave retarded times

$$\tau_\alpha = t - \frac{R}{\alpha}, \qquad \tau_\beta = t - \frac{R}{\beta}. \tag{2.3a,b}$$

2.1 Point Force

The unidirectional point force is a fundamental source of elastic waves. Mathematically, a point force located at position $\mathbf{x}_s$ is represented by the force density (i.e., force per unit volume) function

$$\mathbf{f}(\mathbf{x}, t) = F w(t) \mathbf{a}\, \delta(\mathbf{x} - \mathbf{x}_s), \tag{2.4}$$

where F is a force amplitude scalar (SI units: Newtons), $w(t)$ is a dimensionless source waveform, and **a** is a dimensionless unit vector describing the orientation of the force. The waveform $w(t)$ is typically normalized to unit maximum absolute amplitude. Expressions for the elastic wave radiation from this source are:

Particle velocity:

$$\mathbf{v} = \frac{F}{4\pi\rho}\left\{\frac{1}{\alpha^2 R} w'(\tau_\alpha)(\mathbf{a}\cdot\mathbf{e}_R)\mathbf{e}_R - \frac{1}{\beta^2 R} w'(\tau_\beta)\left[(\mathbf{a}\cdot\mathbf{e}_R)\mathbf{e}_R - \mathbf{a}\right]\right.$$

$$\left. + \left[\frac{1}{\alpha R^2} w(\tau_\alpha) - \frac{1}{\beta R^2} w(\tau_\beta) + \frac{1}{R^3}\int_{\tau_\beta}^{\tau_\alpha} w(\tau)\, d\tau\right]\left[3(\mathbf{a}\cdot\mathbf{e}_R)\mathbf{e}_R - \mathbf{a}\right]\right\}. \qquad (2.5a)$$

Acoustic pressure:

$$p = \frac{F}{4\pi}\left(1 - \frac{4}{3}\gamma^2\right)\left[\frac{1}{\alpha R} w'(\tau_\alpha) + \frac{1}{R^2} w(\tau_\alpha)\right](\mathbf{a}\cdot\mathbf{e}_R). \qquad (2.5b)$$

Particle rotation:

$$\boldsymbol{\omega} = \frac{F}{4\pi\rho\beta^2}\left[\frac{1}{\beta R} w'(\tau_\beta) + \frac{1}{R^2} w(\tau_\beta)\right](\mathbf{a}\times\mathbf{e}_R). \qquad (2.5c)$$

The equations for the elastic radiation contain far-field terms (proportional to $1/R$) and near-field terms (proportional to $1/R^2$). Velocity, pressure, and rotation waveforms change shape from the near-field to the far-field; in the far-field, they have the shape of the derivative of the source force waveform. The acoustic pressure wavefield (propagating with the P-wave speed α) vanishes on the nodal plane defined by $\mathbf{a} \cdot \mathbf{e}_R = 0$. The particle rotation wavefield (propagating with the S-wave speed β) is perpendicular to both $\mathbf{a}$ and $\mathbf{e}_R$, and vanishes along the nodal line $\mathbf{e}_R = \pm\mathbf{a}$. Interestingly, velocity and rotation vectors are orthogonal at all source-receiver distances and directions, i.e., $(\mathbf{v} \cdot \boldsymbol{\omega}) = 0$.

2.2 Point Double-Force

A *finite* double-force consists of two point forces with equal magnitudes F, equal waveforms $w(t)$, oppositely directed orientations $\mathbf{a}$ and $-\mathbf{a}$, and separated in space by the vector $d\mathbf{n}$ (where d is the separation distance and $\mathbf{n}$ is a dimensionless unit vector). In the limit as $d \to 0$ and $F \to \infty$, such that the product $Fd = M$ remains finite, a *point* double-force of strength M is obtained. Note that M has dimension moment (force times distance, or energy; SI unit: Joule). Expressions for the elastic wavefield radiated from the point double-force are derived from the single-force equations via a limiting process. The mathematical details of this process are somewhat involved, and thus are not reproduced here. Only the results are given. First, define the three dimensionless vectors

$$\mathbf{p} = (\mathbf{a}\cdot\mathbf{e}_R)(\mathbf{n}\cdot\mathbf{e}_R)\mathbf{e}_R, \qquad \mathbf{q} = (\mathbf{n}\cdot\mathbf{e}_R)\mathbf{a}, \qquad \mathbf{r} = 6\mathbf{p} - \mathbf{q} - (\mathbf{a}\cdot\mathbf{n})\mathbf{e}_R - (\mathbf{a}\cdot\mathbf{e}_R)\mathbf{n}. \qquad (2.6a,b,c)$$

Then, the formulae for the elastic radiation from a point double-force source are:

Particle velocity:

$$\mathbf{v} = \frac{M}{4\pi\rho}\left\{\frac{1}{\alpha^3 R}w''(\tau_\alpha)\mathbf{p} - \frac{1}{\beta^3 R}w''(\tau_\beta)(\mathbf{p}-\mathbf{q})\right.$$

$$+\frac{1}{\alpha^2 R^2}w'(\tau_\alpha)\mathbf{r} - \frac{1}{\beta^2 R^2}w'(\tau_\beta)(\mathbf{r}-\mathbf{q})$$

$$\left.+\left[\frac{1}{\alpha R^3}w(\tau_\alpha) - \frac{1}{\beta R^3}w(\tau_\beta) + \frac{1}{R^4}\int_{\tau_\beta}^{\tau_\alpha} w(\tau)\,d\tau\right]3(\mathbf{r}-\mathbf{p})\right\}. \qquad (2.7a)$$

Acoustic pressure:

$$p = \frac{M}{4\pi}\left(1-\frac{4}{3}\gamma^2\right)\left\{\frac{1}{\alpha^2 R}w''(\tau_\alpha)(\mathbf{p}\cdot\mathbf{e}_R) + \left[\frac{1}{\alpha R^2}w'(\tau_\alpha) + \frac{1}{R^3}w(\tau_\alpha)\right]\left[3(\mathbf{p}\cdot\mathbf{e}_R) - (\mathbf{a}\cdot\mathbf{n})\right]\right\}. \qquad (2.7b)$$

Particle rotation:

$$\boldsymbol{\omega} = \frac{M}{4\pi\rho\beta^2}\left\{\frac{1}{\beta^2 R}w''(\tau_\beta)(\mathbf{q}\times\mathbf{e}_R) + \left[\frac{1}{\beta R^2}w'(\tau_\beta) + \frac{1}{R^3}w(\tau_\beta)\right]\left[3(\mathbf{q}\times\mathbf{e}_R) - (\mathbf{a}\times\mathbf{n})\right]\right\}. \qquad (2.7c)$$

The radiation from a point double-force consists of far-field (proportional to $1/R$) terms, intermediate-field (proportional to $1/R^2$) terms, and near-field (proportional to $1/R^3$) terms. Also, note that all far-field terms contain the *second* derivative of the source waveform $w(t)$, in contrast with the situation for a point force source. This dimensionless waveform is now interpreted as a moment waveform, rather than a force waveform. Two important special cases of these formulae are described below.

2.2.1 Point Dipole

In the case $\mathbf{n} = \mathbf{a}$, a point dipole of strength M and orientation $\mathbf{a}$ is obtained. Vectors $\mathbf{p}$, $\mathbf{q}$, and $\mathbf{r}$ become

$$\mathbf{p} = (\mathbf{a}\cdot\mathbf{e}_R)^2\mathbf{e}_R, \qquad \mathbf{q} = (\mathbf{a}\cdot\mathbf{e}_R)\mathbf{a}, \qquad \mathbf{r} = 6\mathbf{p} - \mathbf{e}_R - 2\mathbf{q}. \qquad (2.8a,b,c)$$

Expressions for the velocity and pressure are identical to equations (2.7a,b) above (although in the pressure equation one can put $\mathbf{a}\cdot\mathbf{n} = \mathbf{a}\cdot\mathbf{a} = 1$). Since the cross product $\mathbf{a}\times\mathbf{n}$ equals zero, particle rotation simplifies somewhat to:

Particle rotation:

$$\boldsymbol{\omega} = \frac{M}{4\pi\rho\beta^2}\left[\frac{1}{\beta^2 R}w''(\tau_\beta) + \frac{3}{\beta R^2}w'(\tau_\beta) + \frac{3}{R^3}w(\tau_\beta)\right](\mathbf{a}\cdot\mathbf{e}_R)(\mathbf{a}\times\mathbf{e}_R). \qquad (2.9)$$

The rotation now vanishes on the nodal plane $\mathbf{a}\cdot\mathbf{e}_R = 0$ *and* the nodal line $\mathbf{e}_R = \pm\mathbf{a}$.

2.2.2 Point Couple

In the case where **n** is perpendicular to **a** (implying $\mathbf{a} \cdot \mathbf{n} = 0$), a point couple of strength M and orientation $\mathbf{m} = \mathbf{n} \times \mathbf{a}$ is obtained. The mathematical forms of vectors **p** and **q** remain the same, whereas vector **r** reduces to $\mathbf{r} = 6\mathbf{p} - \mathbf{q} - (\mathbf{a} \cdot \mathbf{e}_R)\mathbf{n}$. The expression for the radiated acoustic pressure simplifies to:

Acoustic pressure:

$$p = \frac{M}{4\pi}\left(1 - \frac{4}{3}\gamma^2\right)\left[\frac{1}{\alpha^2 R}w''(\tau_\alpha) + \frac{3}{\alpha R^2}w'(\tau_\alpha) + \frac{3}{R^3}w(\tau_\alpha)\right](\mathbf{a}\cdot\mathbf{e}_R)(\mathbf{n}\cdot\mathbf{e}_R). \tag{2.10}$$

The pressure wavefield now has two orthogonal nodal planes passing through the source position, one perpendicular to **a** and the other perpendicular to **n**.

2.3 Point Double-Couple

Consider the case of *two* point couples located at the same position $\mathbf{x}_s$ in space. Let these couples be characterized by moment scalars M_a and M_b, orientation vectors **a** and **b**, and moment-arm vectors $\mathbf{n}_a$ and $\mathbf{n}_b$, respectively. Note that $\mathbf{a} \cdot \mathbf{n}_a = \mathbf{b} \cdot \mathbf{n}_b = 0$. Both couples are activated by the same source waveform $w(t)$. The velocity, pressure, and rotation generated by this type of source are obtained by superposing the previous expressions for the single-couple. First, define the root-mean-square moment magnitude

$$M_0 = \sqrt{\frac{1}{2}\left(M_a^2 + M_b^2\right)}. \tag{2.11}$$

The moment scalars M_a and M_b can be positive, zero, or negative. However, M_0 is always non-negative. Also, define the three dimensionless vectors

$$\mathbf{p} = \left[\frac{M_a}{M_0}(\mathbf{a}\cdot\mathbf{e}_R)(\mathbf{n}_a\cdot\mathbf{e}_R) + \frac{M_b}{M_0}(\mathbf{b}\cdot\mathbf{e}_R)(\mathbf{n}_b\cdot\mathbf{e}_R)\right]\mathbf{e}_R, \tag{2.12a}$$

$$\mathbf{q} = \frac{M_a}{M_0}(\mathbf{n}_a\cdot\mathbf{e}_R)\mathbf{a} + \frac{M_b}{M_0}(\mathbf{n}_b\cdot\mathbf{e}_R)\mathbf{b}, \tag{2.12b}$$

$$\mathbf{r} = 6\mathbf{p} - \mathbf{q} - \frac{M_a}{M_0}(\mathbf{a}\cdot\mathbf{e}_R)\mathbf{n}_a - \frac{M_b}{M_0}(\mathbf{b}\cdot\mathbf{e}_R)\mathbf{n}_b. \tag{2.12c}$$

Then, the elastic wavefield radiated by the set of two coincident point couples has the same mathematical forms as those radiated from the single-couple, viz:

Particle velocity:

$$\mathbf{v} = \frac{M_0}{4\pi\rho}\left\{\frac{1}{\alpha^3 R}w''(\tau_\alpha)\mathbf{p} - \frac{1}{\beta^3 R}w''(\tau_\beta)(\mathbf{p}-\mathbf{q})\right.$$

$$+\frac{1}{\alpha^2 R^2}w'(\tau_\alpha)\mathbf{r} - \frac{1}{\beta^2 R^2}w'(\tau_\beta)(\mathbf{r}-\mathbf{q})$$

$$\left.+\left[\frac{1}{\alpha R^3}w(\tau_\alpha) - \frac{1}{\beta R^3}w(\tau_\beta) + \frac{1}{R^4}\int_{\tau_\beta}^{\tau_\alpha} w(\tau)\,d\tau\right]3(\mathbf{r}-\mathbf{p})\right\}. \qquad (2.13a)$$

Acoustic pressure:

$$p = \frac{M_0}{4\pi}\left(1-\frac{4}{3}\gamma^2\right)\left[\frac{1}{\alpha^2 R}w''(\tau_\alpha) + \frac{3}{\alpha R^2}w'(\tau_\alpha) + \frac{3}{R^3}w(\tau_\alpha)\right](\mathbf{p}\cdot\mathbf{e}_R). \qquad (2.13b)$$

Particle rotation:

$$\boldsymbol{\omega} = \frac{M_0}{4\pi\rho\beta^2}\left\{\frac{1}{\beta^2 R}w''(\tau_\beta)(\mathbf{q}\times\mathbf{e}_R) + \left[\frac{1}{\beta R^2}w'(\tau_\beta) + \frac{1}{R^3}w(\tau_\beta)\right]\left[3(\mathbf{q}\times\mathbf{e}_R) + \mathbf{m}_a + \mathbf{m}_b\right]\right\}. \qquad (2.13c)$$

In the last expression, $\mathbf{m}_a = (\mathbf{n}_a \times \mathbf{a})$ and $\mathbf{m}_b = (\mathbf{n}_b \times \mathbf{b})$ are unit magnitude moment-direction vectors. There are two important special cases to consider.

2.3.1 Double-Couple With Moment

Suppose that $M_b = M_a = M$, $\mathbf{b} = \pm\mathbf{n}_a$, and $\mathbf{n}_b = \mp\mathbf{a}$. In this case, the pair of couples exerts a net moment on the elastic medium about an axis through the source location. Vectors **p** and **r** vanish, and **q** becomes

$$\mathbf{q} = \frac{M}{|M|}\left[(\mathbf{n}_a\cdot\mathbf{e}_R)\mathbf{a} - (\mathbf{a}\cdot\mathbf{e}_R)\mathbf{n}_a\right] = \frac{M}{|M|}\left[(\mathbf{n}_a\times\mathbf{a})\times\mathbf{e}_R\right] = \frac{M}{|M|}(\mathbf{m}\times\mathbf{e}_R), \qquad (2.14)$$

where $\mathbf{m} = \mathbf{n}_a \times \mathbf{a}$. The velocity and rotation vectors reduce to:

Particle velocity:

$$\mathbf{v} = \frac{M}{4\pi\rho}\left[\frac{1}{\beta^3 R}w''(\tau_\beta) + \frac{1}{\beta^2 R^2}w'(\tau_\beta)\right](\mathbf{m}\times\mathbf{e}_R), \qquad (2.15a)$$

Particle rotation:

$$\boldsymbol{\omega} = \frac{M}{4\pi\rho\beta^2}\left\{\frac{1}{\beta^2 R}w''(\tau_\beta)[(\mathbf{m}\cdot\mathbf{e}_R)\mathbf{e}_R - \mathbf{m}] + \left[\frac{1}{\beta R^2}w'(\tau_\beta) + \frac{1}{R^3}w(\tau_\beta)\right][3(\mathbf{m}\cdot\mathbf{e}_R)\mathbf{e}_R - \mathbf{m}]\right\}, \tag{2.15b}$$

and the pressure p vanishes. This source generates only shear waves. The velocity vector is perpendicular to both $\mathbf{m}$ and $\mathbf{e}_R$, and vanishes in the source-to-receiver directions $\mathbf{e}_R = \pm\mathbf{m}$. Hence, the vector $\mathbf{m}$ may be regarded as an axis about which the motion takes place. Other names for the double-couple with net moment are "point center of rotation" or "point torque".

2.3.2 Double-Couple Without Moment

Suppose that the two point couples have identical magnitudes and oppositely directed moments, so that the net moment of the pair vanishes. This occurs if $M_b = M_a = M$, $\mathbf{b} = \pm\mathbf{n}_a$, and $\mathbf{n}_b = \pm\mathbf{a}$. Vectors $\mathbf{p}$, $\mathbf{q}$, and $\mathbf{r}$ become

$$\mathbf{p} = \frac{M}{|M|}2(\mathbf{a}\cdot\mathbf{e}_R)(\mathbf{n}_a\cdot\mathbf{e}_R)\mathbf{e}_R, \qquad \mathbf{q} = \frac{M}{|M|}[(\mathbf{n}_a\cdot\mathbf{e}_R)\mathbf{a} + (\mathbf{a}\cdot\mathbf{e}_R)\mathbf{n}_a], \qquad \mathbf{r} = 6\mathbf{p} - 2\mathbf{q}, \tag{2.16a,b,c}$$

and the particle velocity and acoustic pressure can be expressed solely in terms of $\mathbf{p}$ and $\mathbf{q}$. The radiated elastic wavefield is given by

Particle velocity:

$$\begin{aligned}\mathbf{v} = \frac{|M|}{4\pi\rho}\Bigg\{&\frac{1}{\alpha^3 R}w''(\tau_\alpha)\mathbf{p} - \frac{1}{\beta^3 R}w''(\tau_\beta)(\mathbf{p}-\mathbf{q}) \\ &+ \frac{1}{\alpha^2 R^2}w'(\tau_\alpha)2(3\mathbf{p}-\mathbf{q}) - \frac{1}{\beta^2 R^2}w'(\tau_\beta)3(2\mathbf{p}-\mathbf{q}) \\ &+ \left[\frac{1}{\alpha R^3}w(\tau_\alpha) - \frac{1}{\beta R^3}w(\tau_\beta) + \frac{1}{R^4}\int_{\tau_\beta}^{\tau_\alpha} w(\tau)\,d\tau\right]3(5\mathbf{p}-2\mathbf{q})\Bigg\}.\end{aligned} \tag{2.17a}$$

Acoustic pressure:

$$p = \frac{M}{4\pi}\left(1 - \frac{4}{3}\gamma^2\right)\left[\frac{1}{\alpha^2 R}w''(\tau_\alpha) + \frac{3}{\alpha R^2}w'(\tau_\alpha) + \frac{3}{R^3}w(\tau_\alpha)\right]2(\mathbf{a}\cdot\mathbf{e}_R)(\mathbf{n}_a\cdot\mathbf{e}_R). \tag{2.17b}$$

Particle rotation:

$$\boldsymbol{\omega} = \frac{M}{4\pi\rho\beta^2}\left[\frac{1}{\beta^2 R}w''(\tau_\beta) + \frac{3}{\beta R^2}w'(\tau_\beta) + \frac{3}{R^3}w(\tau_\beta)\right]\left[(\mathbf{a}\cdot\mathbf{e}_R)\mathbf{n}_a + (\mathbf{n}_a\cdot\mathbf{e}_R)\mathbf{a}\right]\times\mathbf{e}_R . \qquad (2.17c)$$

Careful examination reveals that the P-wave radiation generated by the point double-couple without moment is exactly *twice* that generated by the single-couple. The difference in the two wavefields is contained entirely in the far-field and intermediate-field S-wave radiation.

An alternate representation of the double-couple without moment in terms of orthogonal tension and compression dipoles is illustrative. Define the two orthogonal unit vectors

$$\mathbf{t} = \frac{1}{\sqrt{2}}(\mathbf{n}_a + \mathbf{a}), \qquad \mathbf{c} = \frac{1}{\sqrt{2}}(\mathbf{n}_a - \mathbf{a}). \qquad (2.18a,b)$$

Vectors **p** and **q** for the double-couple without moment can be expressed as

$$\mathbf{p} = \frac{M}{|M|}\left[(\mathbf{t}\cdot\mathbf{e}_R)^2 - (\mathbf{c}\cdot\mathbf{e}_R)^2\right]\mathbf{e}_R, \qquad \mathbf{q} = \frac{M}{|M|}\left[(\mathbf{t}\cdot\mathbf{e}_R)\mathbf{t} - (\mathbf{c}\cdot\mathbf{e}_R)\mathbf{c}\right], \qquad (2.19a,b)$$

and these can be inserted into the above formulae for the velocity and pressure radiated by this source. However, these forms for vectors **p** and **q** (and thus **r** = 6**p** - 2**q**) are identical to those associated with the superposition of two orthogonal force dipoles with equal strengths M, one in tension (with orientation **t**) and the other in compression (with orientation **c**). Hence, this particular superposition constitutes an equivalent description of the point double-couple without moment.

2.4 Point Tri-Dipole

A reasonably general source force configuration consists of three dipoles with arbitrary orientations (**a**, **b**, **c**) and strengths (M_a, M_b, M_c) located at the same point in space. The elastic waves radiated from this type of source are obtained by superposing the expressions for the single force dipole. The root-mean-square magnitude of the three moment scalars is

$$M_0 = \sqrt{\frac{1}{3}\left(M_a^2 + M_b^2 + M_c^2\right)}. \qquad (2.20)$$

Also, define three dimensionless vectors as

$$\mathbf{p} = \left[\frac{M_a}{M_0}(\mathbf{a}\cdot\mathbf{e}_R)^2 + \frac{M_b}{M_0}(\mathbf{b}\cdot\mathbf{e}_R)^2 + \frac{M_c}{M_0}(\mathbf{c}\cdot\mathbf{e}_R)^2\right]\mathbf{e}_R, \qquad (2.21a)$$

$$\mathbf{q} = \frac{M_a}{M_0}(\mathbf{a}\cdot\mathbf{e}_R)\mathbf{a} + \frac{M_b}{M_0}(\mathbf{b}\cdot\mathbf{e}_R)\mathbf{b} + \frac{M_c}{M_0}(\mathbf{c}\cdot\mathbf{e}_R)\mathbf{c}, \qquad (2.21b)$$

$$\mathbf{r} = 6\mathbf{p} - 2\mathbf{q} - \left[\frac{M_a + M_b + M_c}{M_0}\right]\mathbf{e}_R . \tag{2.21c}$$

Then, the particle velocity and acoustic pressure seismograms for the tri-dipole source are given by

Particle velocity:

$$\mathbf{v} = \frac{M_0}{4\pi\rho}\left\{\frac{1}{\alpha^3 R}w''(\tau_\alpha)\mathbf{p} - \frac{1}{\beta^3 R}w''(\tau_\beta)(\mathbf{p}-\mathbf{q})\right.$$

$$+\frac{1}{\alpha^2 R^2}w'(\tau_\alpha)\mathbf{r} - \frac{1}{\beta^2 R^2}w'(\tau_\beta)(\mathbf{r}-\mathbf{q})$$

$$\left.+\left[\frac{1}{\alpha R^3}w(\tau_\alpha) - \frac{1}{\beta R^3}w(\tau_\beta) + \frac{1}{R^4}\int_{\tau_\beta}^{\tau_\alpha} w(\tau)\,d\tau\right]3(\mathbf{r}-\mathbf{p})\right\}. \tag{2.22a}$$

Acoustic pressure:

$$p = \frac{M_0}{4\pi}\left(1 - \frac{4}{3}\gamma^2\right)\left\{\frac{1}{\alpha^2 R}w''(\tau_\alpha)(\mathbf{p}\cdot\mathbf{e}_R)\right.$$

$$\left.+\left[\frac{3}{\alpha R^2}w'(\tau_\alpha) + \frac{3}{R^3}w(\tau_\alpha)\right]\left[(\mathbf{p}\cdot\mathbf{e}_R) - \frac{M_a + M_b + M_c}{3M_0}\right]\right\}. \tag{2.22b}$$

Particle rotation:

$$\boldsymbol{\omega} = \frac{M_0}{4\pi\rho\beta^2}\left[\frac{1}{\beta^2 R}w''(\tau_\beta) + \frac{3}{\beta R^2}w'(\tau_\beta) + \frac{3}{R^3}w(\tau_\beta)\right](\mathbf{q}\times\mathbf{e}_R). \tag{2.22c}$$

Note that the relevant expressions for the double-couple with no net moment are obtained by taking $M_a = M$, $M_b = -M$, $M_c = 0$, and $\mathbf{a}\cdot\mathbf{b} = 0$. Vectors **a** and **b** are then interpreted as unit tension and compression vectors for the two orthogonal dipoles, respectively. Once again, the remarkable orthogonality property $(\mathbf{v}\cdot\boldsymbol{\omega}) = 0$ is evident.

2.4.1 Point Source of Compression

A point source of compression (i.e., an explosion) can be represented by three mutually perpendicular tension dipoles of equal strength. Hence, this source is a special case of the tri-dipole source described above. If (**a**, **b**, **c**) is an orthonormal triad of vectors and $M_a = M_b = M_c = M$, then $\mathbf{p} = \mathbf{q} = \mathbf{r} = \mathrm{sgn}(M)\,\mathbf{e}_R$ and formulae (2.22) reduce to:

Particle velocity:

$$\mathbf{v} = \frac{M}{4\pi\rho}\left[\frac{1}{\alpha^3 R}w''(\tau_\alpha) + \frac{1}{\alpha^2 R^2}w'(\tau_\alpha)\right]\mathbf{e}_R, \tag{2.23a}$$

Acoustic pressure:

$$p = \frac{M}{4\pi}\left(1 - \frac{4}{3}\gamma^2\right)\frac{1}{\alpha^2 R}w''(\tau_\alpha), \tag{2.23b}$$

and the rotation ω vanishes. Note that the velocity is strictly radial and propagates with the P-wave speed α. The pressure amplitude is inversely proportional to the radial distance R, and the pressure wavefield has no nodal planes.

3.0 ACOUSTIC MEDIUM

A homogeneous and isotropic acoustic wholespace is characterized by shear wave speed β equal to zero. In the limiting case $\beta \rightarrow 0$, the above expressions for acoustic pressure p are well defined (the multiplicative factor $1-(4/3)\gamma^2$ approaches unity; recall that $\gamma \equiv \beta/\alpha$). Limiting expressions for the particle velocity vector **v** are obtained as follows. For non-zero radius R, the S-wave retarded time $\tau_\beta = t - R/\beta$ approaches $-\infty$ as $\beta \rightarrow 0$. If the two conditions

$$\lim_{\beta\to 0} \frac{1}{\beta} w(\tau_\beta) = 0, \qquad \lim_{\beta\to 0} \frac{1}{\beta^2} w'(\tau_\beta) = 0,$$

hold, then the equation for the particle velocity vector radiated by the point force source reduces to

Point force:

$$\mathbf{v} = \frac{F}{4\pi\rho}\left\{\frac{1}{\alpha^2 R} w'(\tau_\alpha)(\mathbf{a}\cdot\mathbf{e}_R)\mathbf{e}_R + \left[\frac{1}{\alpha R^2} w(\tau_\alpha) + \frac{1}{R^3}\int_{-\infty}^{\tau_\alpha} w(\tau)\,d\tau\right]\left[3(\mathbf{a}\cdot\mathbf{e}_R)\mathbf{e}_R - \mathbf{a}\right]\right\}. \tag{3.1}$$

If the additional condition

$$\lim_{\beta\to 0} \frac{1}{\beta^3} w''(\tau_\beta) = 0,$$

is satisfied, then the limiting equation for the particle velocity vector radiated by a point moment source is

Point moment:

$$\mathbf{v} = \frac{M_0}{4\pi\rho}\left\{\frac{1}{\alpha^3 R} w''(\tau_\alpha)\mathbf{p} + \frac{1}{\alpha^2 R^2} w'(\tau_\alpha)\mathbf{r} + \left[\frac{1}{\alpha R^3} w(\tau_\alpha) + \frac{1}{R^4}\int_{-\infty}^{\tau_\alpha} w(\tau)\,d\tau\right] 3(\mathbf{r}-\mathbf{p})\right\}. \tag{3.2}$$

The formulae appropriate for a force dipole, force couple, double-couple (with or without moment), tri-dipole, explosion, etc. are all special cases of this equation, provided the appropriate forms of the vectors **p**, **q**, and **r** are used. In particular, for the tri-dipole source, if vectors (**a**,**b**,**c**) are orthonormal and $M_a = M_b = M_c = M$, the above expression becomes

Point source of compression:

$$\mathbf{v} = \frac{M}{4\pi\rho}\left[\frac{1}{\alpha^3 R} w''(\tau_\alpha) + \frac{1}{\alpha^2 R^2} w'(\tau_\alpha)\right]\mathbf{e}_R. \tag{3.3}$$

Interestingly, the particle velocity radiated by an explosive source is the same for an elastic or acoustic wholespace. The pressure, however, differs by the factor $1-(4/3)\gamma^2$.

Since shear waves do not propagate within an ideal fluid, the particle rotation vector ω must reduce to zero. Curiously, the mathematical conditions required for vanishing rotation are more stringent than those used to obtain the particle velocity in an acoustic medium. In particular, for a force source, the limits

$$\lim_{\beta \to 0} \frac{1}{\beta^2} w(\tau_\beta) = 0, \qquad \lim_{\beta \to 0} \frac{1}{\beta^3} w'(\tau_\beta) = 0,$$

imply that rotation $\omega \to \mathbf{0}$. For a moment source, the additional condition

$$\lim_{\beta \to 0} \frac{1}{\beta^4} w''(\tau_\beta) = 0,$$

is required for vanishing ω.

All of the above limits certainly hold if the source wavelet $w(t)$ is causal (i.e., $w(t) = 0$ for $t < 0$). However, they are also valid in the case of a noncausal wavelet that vanishes sufficiently rapidly as t approaches $-\infty$. For example, a Ricker wavelet with peak frequency f_p is given by

$$w(t) = \left[1 - 2(\pi f_p t)^2\right] \exp\left[-(\pi f_p t)^2\right]. \tag{3.4}$$

For large $|t|$, the nth derivative of $w(t)$ is dominated by a term proportional to $(\pi f_p t)^{n+2} \exp[-(\pi f_p t)^2]$. As time $t \to -\infty$, this term vanishes rapidly enough to ensure that all of the above limits are satisfied.

4.0 FAR-FIELD APPROXIMATION

In the above equations, the far-field acoustic pressure is in-phase with the far-field radial particle velocity. Let $v_R = \mathbf{v} \cdot \mathbf{e}_R$ be the radial component of the particle velocity vector. Also, let the subscript "far" denote far-field quantities (i.e., proportional to $1/R$). Then

$$\left.\frac{p}{v_R}\right|_{\text{far}} = \rho\alpha\left(1 - \frac{4}{3}\gamma^2\right). \tag{4.1}$$

For an isotropic elastic medium, $0 \le \gamma \le \sqrt{3}/2 \approx 0.866$ (assuming materials with negative Poisson ratio are allowed). Hence, the right hand side of the above expression is non-negative, implying that far-field pressure and radial particle velocity are in-phase. In the limiting case of a fluid medium (shear wave speed $\beta \to 0$ implying $\gamma \to 0$), the ratio of the far-field pressure to far-field radial particle velocity equals the acoustic impedance $\rho\alpha$ of the medium.

The above "in-phase" relation between far-field pressure and radial particle velocity is not limited to *point* sources of elastic waves in a homogeneous and isotropic wholespace. In particular, it also applies in the case of a *line* source of finite length, activated as a force, torque, or pressure source (Aldridge, 1998). Other examples can probably be found.

5.0 MOMENT TENSOR REPRESENTATION

The point moment sources described above are characterized by a combination of force dipoles or force couples. An alternative, but equivalent, representation of this type of source involves the moment density tensor

$$m_{ij}(\mathbf{x},t) = -M_0 w(t) a_{ij} \delta(\mathbf{x} - \mathbf{x}_s), \tag{5.1}$$

where M_0 is a moment amplitude scalar, $w(t)$ is a dimensionless source waveform (normalized to unit maximum absolute amplitude), and a_{ij} are the components of a dimensionless second-rank tensor. The moment density tensor has physical dimension of moment per volume, or energy per volume (SI unit: Joule/m^3), or pressure (SI unit: Pascal), Consider the most general case discussed so far, where three point double-forces are superposed at the same position in space. Then, the nine components a_{ij} are defined by

$$a_{xx} = \frac{M_a}{M_0} a_x n_x^a + \frac{M_b}{M_0} b_x n_x^b + \frac{M_c}{M_0} c_x n_x^c, \tag{5.2a}$$

$$a_{xy} = \frac{M_a}{M_0} a_x n_y^a + \frac{M_b}{M_0} b_x n_y^b + \frac{M_c}{M_0} c_x n_y^c, \tag{5.2b}$$

$$a_{xz} = \frac{M_a}{M_0} a_x n_z^a + \frac{M_b}{M_0} b_x n_z^b + \frac{M_c}{M_0} c_x n_z^c, \tag{5.2c}$$

$$a_{yx} = \frac{M_a}{M_0} a_y n_x^a + \frac{M_b}{M_0} b_y n_x^b + \frac{M_c}{M_0} c_y n_x^c, \tag{5.2d}$$

$$a_{yy} = \frac{M_a}{M_0} a_y n_y^a + \frac{M_b}{M_0} b_y n_y^b + \frac{M_c}{M_0} c_y n_y^c, \tag{5.2e}$$

$$a_{yz} = \frac{M_a}{M_0} a_y n_z^a + \frac{M_b}{M_0} b_y n_z^b + \frac{M_c}{M_0} c_y n_z^c, \tag{5.2f}$$

$$a_{zx} = \frac{M_a}{M_0} a_z n_x^a + \frac{M_b}{M_0} b_z n_x^b + \frac{M_c}{M_0} c_z n_x^c, \tag{5.2g}$$

$$a_{zy} = \frac{M_a}{M_0} a_z n_y^a + \frac{M_b}{M_0} b_z n_y^b + \frac{M_c}{M_0} c_z n_y^c, \tag{5.2h}$$

$$a_{zz} = \frac{M_a}{M_0} a_z n_z^a + \frac{M_b}{M_0} b_z n_z^b + \frac{M_c}{M_0} c_z n_z^c, \tag{5.2i}$$

where superscripts, rather than subscripts, are used to identify the three moment-arm vectors $\mathbf{n}_a$, $\mathbf{n}_b$, and $\mathbf{n}_c$, and M_0 is the rms value of the three moment amplitude scalars M_a, M_b, and M_c. Expressions appropriate for the dipole, couple, double-couple (with or without moment), tri-dipole, explosion, etc. are all special cases of these formulae. Note that the tensor a_{ij} is not necessarily symmetric. Let the symbol **A** refer to the 3 × 3 tensor with components a_{ij}. Then, define the three vectors

$$\mathbf{p} = \left(\mathbf{e}_R^T \mathbf{A} \mathbf{e}_R\right)\mathbf{e}_R, \qquad \mathbf{q} = \mathbf{A}\mathbf{e}_R, \qquad \mathbf{r} = \left[6\left(\mathbf{e}_R^T \mathbf{A} \mathbf{e}_R\right) - \mathrm{tr}(\mathbf{A})\right]\mathbf{e}_R - \left[\mathbf{A} + \mathbf{A}^T\right]\mathbf{e}_R, \tag{5.3a,b,c}$$

where $\mathrm{tr}(\mathbf{A}) = a_{xx} + a_{yy} + a_{zz}$ is the trace of **A**, and the superscript T denotes transposition. Clearly, vectors **p** and **q** are related via $\mathbf{p} = (\mathbf{q} \cdot \mathbf{e}_R)\mathbf{e}_R$, and **r** can be written as

$$\mathbf{r} = 6\mathbf{p} - \mathrm{tr}(\mathbf{A})\mathbf{e}_R - \mathbf{q} - \mathbf{A}^T\mathbf{e}_R. \tag{5.3d}$$

In terms of the above vectors, the elastic wavefield radiated by a point moment source is described by the now-familiar formulae

Particle velocity:

$$\begin{aligned}\mathbf{v} = \frac{M_0}{4\pi\rho}\Bigg\{ & \frac{1}{\alpha^3 R} w''(\tau_\alpha)\mathbf{p} - \frac{1}{\beta^3 R} w''(\tau_\beta)(\mathbf{p}-\mathbf{q}) \\ & + \frac{1}{\alpha^2 R^2} w'(\tau_\alpha)\mathbf{r} - \frac{1}{\beta^2 R^2} w'(\tau_\beta)(\mathbf{r}-\mathbf{q}) \\ & + \left[\frac{1}{\alpha R^3} w(\tau_\alpha) - \frac{1}{\beta R^3} w(\tau_\beta) + \frac{1}{R^4}\int_{\tau_\beta}^{\tau_\alpha} w(\tau)\, d\tau\right] 3(\mathbf{r}-\mathbf{p})\Bigg\}.\end{aligned} \tag{5.4a}$$

Acoustic pressure:

$$p = \frac{M_0}{4\pi}\left(1 - \frac{4}{3}\gamma^2\right)\left\{\frac{1}{\alpha^2 R} w''(\tau_\alpha)(\mathbf{p}\cdot\mathbf{e}_R) + \left[\frac{1}{\alpha R^2} w'(\tau_\alpha) + \frac{1}{R^3} w(\tau_\alpha)\right]\left[3(\mathbf{p}\cdot\mathbf{e}_R) - \mathrm{tr}(\mathbf{A})\right]\right\}, \tag{5.4b}$$

Particle rotation:

$$\boldsymbol{\omega} = \frac{M_0}{4\pi\rho\beta^2}\left[\frac{1}{\beta^2 R} w''(\tau_\beta) + \frac{3}{\beta R^2} w'(\tau_\beta) + \frac{3}{R^3} w(\tau_\beta)\right](\mathbf{q}\times\mathbf{e}_R). \tag{5.4c}$$

Interestingly, the above formulae imply that the compressional wave radiation generated by a point moment source depends *only* on the symmetric part of the tensor **A**. The symmetric and anti-symmetric parts of **A** are given by

$$\mathbf{A}_s = \frac{1}{2}\left(\mathbf{A} + \mathbf{A}^T\right), \qquad \mathbf{A}_a = \frac{1}{2}\left(\mathbf{A} - \mathbf{A}^T\right),$$

respectively. Substituting $\mathbf{A} = \mathbf{A}_s + \mathbf{A}_a$ into the expressions for vectors **p**, **q**, and **r** gives

$$\mathbf{p} = \left(\mathbf{e}_R^T \mathbf{A}_s \mathbf{e}_R\right)\mathbf{e}_R, \qquad \mathbf{q} = \mathbf{A}_s \mathbf{e}_R + \mathbf{A}_a \mathbf{e}_R, \qquad \mathbf{r} = \left[6\left(\mathbf{e}_R^T \mathbf{A}_s \mathbf{e}_R\right) - \mathrm{tr}\left(\mathbf{A}_s\right)\right]\mathbf{e}_R - 2\mathbf{A}_s \mathbf{e}_R, \qquad (5.5a,b,c)$$

because the inner product $\mathbf{e}_R{}^T \mathbf{A}_a \mathbf{e}_R$ and the trace $\mathrm{tr}(\mathbf{A}_a)$ vanish. Hence, if **A** is purely anti-symmetric, then vectors **p** and **r** are zero, and no P-waves are radiated by the source. Moreover, the S-waves are polarized normal to the source-to-receiver direction $\mathbf{e}_R$, since $\mathbf{q} \cdot \mathbf{e}_R = \mathbf{e}_R{}^T \mathbf{A}_s \mathbf{e}_R + \mathbf{e}_R{}^T \mathbf{A}_a \mathbf{e}_R = 0 + 0$. The point torque source, for which $a_{ij} = a_i n_j - a_j n_i$, is an example.

6.0 NUMERICAL ALGORITHM

Closed-form mathematical expressions for particle velocity **v**, acoustic pressure p, and particle rotation ω are amenable to straightforward numerical evaluation. For force sources [i.e., equation (2.4)], equations (2.5a,b,c) are evaluated. For moment sources [i.e., equation (5.1)], equations (5.4a,b,c) are evaluated. Vectors **p**, **q**, and **r** in the latter expressions are obtained from the moment tensor description given by equations (5.3a,b,c). In the special case of an acoustic medium ($\beta = 0$), velocity wavefields for force and moment sources are calculated via formulae (3.1) and (3.2), respectively, and rotation wavefields are set equal to zero. The algorithm does not verify that a source wavelet $w(t)$ satisfies the limiting conditions appropriate for an ideal fluid detailed in section 3.0. As indicated previously, all expressions for acoustic pressure remain usable in the limiting case $\beta \rightarrow 0$.

A file describing the geometric distribution of sources and receivers, as well as other defining characteristics, is input to the algorithm. Required information for each point source includes:

Force source: three-dimensional position coordinates (x_s, y_s, z_s); magnitude scalar F; unit orientation vector **a**; waveform $w(t)$.

Moment source: three-dimensional position coordinates (x_s, y_s, z_s); magnitude scalar M; orientation tensor **A**; waveform $w(t)$.

The elements of tensor **A** for a moment source are obtained from equations (5.2a) through (5.2i) in terms of the magnitudes and orientations of three spatially coincident force dipoles or couples. Multiple point sources, of various types, positions, magnitudes, orientations, and waveforms, may be activated simultaneously.

For each source, a discretely sampled waveform $w(t_n)$ with $t_n = t_{\min} + (n\text{-}1)\Delta t$ for $n = 1 \rightarrow N$ is utilized. The expressions for velocity, pressure, and rotation require the waveform and its derivatives to be evaluated at the P-wave and S-wave retarded times τ_α and τ_β, which may not coincide with any sample instant t_n. Numerical values are obtained between sample times by locally approximating the sampled waveform $w(t_n)$ with a cubic polynomial. In general, the resulting estimates of w, w', and w'' possess fourth-order, third-order, and second-order accuracy in the temporal discretization interval Δt, respectively (Fornberg, 1988). Mathematical details of the technique are presented in Appendix A. Additionally, the integral of the source waveform between the S-wave and P-wave retarded times is needed in the formulae. The "alternative extended Simpson's rule" (Press *et al.*, 1986, p. 108) is used for numerical quadrature, yielding high-order accuracy in the sample interval Δt.

Required input information regarding point receivers includes:

Velocity or rotation sensor: three-dimensional position coordinates (x_r, y_r, z_r); sensitivity scalar S; unit orientation vector **d**.

Pressure sensor: three-dimensional position coordinates (x_r, y_r, z_r); sensitivity scalar S.

Multiple point receivers, with various positions, sensitivities, and orientations may also be active simultaneously. Receivers may be deployed in an arbitrary (i.e., fully three-dimensional) configuration; there is no restriction to uniform spacing or gridding. A velocity or rotation sensor may be oriented in any direction **d**; there is no restriction to orientations parallel to the x, y, or z coordinate axes. Components of the velocity and rotation vectors along a receiver sensitivity axis are obtained by

evaluating the dot products $(\mathbf{v} \cdot \mathbf{d})$ and $(\omega \cdot \mathbf{d})$, respectively. Finally, the sensitivity scalar S is merely a multiplicative factor designed to convert the calculated wavefield quantity (velocity, rotation, or pressure) to preferred numerical values or units. Wavefield quantities are not convolved with receiver impulse responses.

7.0 SYNTHETIC SEISMOGRAMS

7.1 Earth Model and Recording Geometry

The earth model used in subsequent calculations consists of a homogeneous and isotropic elastic wholespace with P-wave speed $\alpha = 2000$ m/s, S-wave speed $\beta = 1000$ m/s, and mass density $\rho = 2000$ kg/m^3. The data acquisition geometry simulates a crosswell recording configuration. For most of the examples, various point sources are located at $(x_s, y_s, z_s) = (0, 0, 0)$ m. Forty one receivers, separated by a 5 m depth interval, are distributed in a vertical borehole at $(x_r, y_r) = (100, 0)$ m. Vertical receiver positions range from $z_r = -100$ m to $z_r = +100$ m relative to the source. Hence, raypaths to far offset receivers are oriented at ±45° with respect to horizontal. The depth of this crosswell experiment is considered great enough so that reflected energy from the stress-free surface of the earth does not arrive at the receivers within the recording time window.

7.2 Sources and Receivers

Various types of point sources are modeled: i) unidirectional forces oriented in the $+x$, $+y$, and $+z$ directions, ii) isotropic explosion, iii) explosion combined with a vertical force dipole, iv) unidirectional torques oriented in the $+x$, $+y$, and $+z$ directions, v) double-couple without moment, vi) rotating horizontal point force, and vii) spatially distributed arrays of point forces.

For all examples, the source waveform is a Berlage wavelet (Aldridge, 1990). This waveform possesses advantages of causality and differentiability. A Berlage wavelet defined by main frequency $f_0 = \omega_0/2\pi$, damping factor h, time-exponent n, and initial phase angle θ_0 is given by

$$w(t) = AH(t)(\omega_0 t)^n \exp(-h\omega_0 t)\cos(\omega_0 t + \theta_0), \tag{7.1}$$

where $H(t)$ is the Heaviside unit step function. The dimensionless factor A is usually chosen so that the maximum absolute amplitude of $w(t)$ is unity. Figure 1 depicts a Berlage wavelet with $f_0 = 80$ Hz, $h = 1$, $n = 3$, and $\theta_0 = -\pi/2$ radians. Additionally, plots of the first and second derivatives of the wavelet (also normalized to unit maximum absolute value) are given. For point force sources, the far-field velocity, pressure, and rotation waveforms are given by $w'(t)$. For point moment sources, far-field waveforms equal $w''(t)$.

The Fourier spectrum of the Berlage wavelet is

$$W(f) = \frac{A\Gamma(n+1)}{4\pi f_0} e^{-i(n+1)\pi/2}\left\{e^{+i\theta_0}\left[\frac{f}{f_0} - 1 - ih\right]^{-(n+1)} + e^{-i\theta_0}\left[\frac{f}{f_0} + 1 - ih\right]^{-(n+1)}\right\}, \tag{7.2}$$

where $\Gamma(x)$ is the gamma function and $i = \sqrt{-1}$. Thus, for $f >> f_0$, the amplitude spectrum is proportional to $1/f^{n+1}$. Figure 2 displays the frequency amplitude spectrum of the same Berlage wavelet plotted in figure 1, as well as the amplitude spectra of its first and second derivatives. Clearly, differentiation boosts the high frequency content of the spectrum.

The wavelengths of compressional and shear waves propagating at the P and S wavespeeds are $\lambda_\alpha = \alpha/f$ and $\lambda_\beta = \beta/f$, where f is frequency. For $f = 80$ Hz, these are $\lambda_\alpha = 25$ m and $\lambda_\beta = 12.5$ m. Hence, for

frequencies at and near the mode of the source amplitude spectrum, the receivers are located in the far-field. At lower frequencies (say $f = 20$ Hz) the nearest receiver is only 1 compressional and 2 shear wavelengths distant from the source, and near-field effects are relatively more important.

Receivers record the three Cartesian components of the particle velocity vector (v_x, v_y, v_z) and rotation vector (ω_x, ω_y, ω_z), and the acoustic pressure (p). Computed traces are not convolved with any receiver impulse responses. Trace duration is 150 ms and time sample interval is 0.5 ms. In accordance with borehole seismology convention, traces are plotted with time increasing in the horizontal direction. Shaded lobes of the traces represent positive excursions.

7.3 Example 1: Unidirectional Forces

Figures 3, 4, and 5 illustrate three-component particle velocity seismograms generated by point forces oriented in the $+x$, $+y$, and $+z$ directions, respectively. P-wave and S-wave arrivals with hyperbolic moveout trajectories across the receiver spread are clearly evident. For the receiver located at the same depth as the source ($z_r = z_s = 0$ m), onsets of these arrivals occur at 50 ms and 100 ms, respectively. These figures display a "nine component seismic survey" for the crosswell recording geometry: three orthogonal force sources recorded by three orthogonal geophones.

Figures 6, 7, and 8 depict three-component particle rotation seismograms generated by the same set of point forces. Only shear wave arrivals exist. Comparing rotation and velocity trace panels illustrates the orthogonality condition $(\mathbf{v} \cdot \omega) = 0$.

Figure 9 indicates that the pressure wavefield generated by the three force sources propagates with the compresssional wave speed α. There are no shear wave arrivals on the pressure seismograms.

7.4 Example 2: Isotropic Explosion

A point source of compression (i.e., an isotropic explosion) generates only radially polarized P-waves. Hence, there is no arrival on the tranvserse (v_y) component traces in figure 10, and particle rotation traces are identically zero in figure 11. The acoustic pressure arrival in figure 12 propagates with the P-wave speed α, and exhibits no amplitude nodes.

7.5 Example 3: Explosion Plus Vertical Dipole

The elastic wavefield produced by an explosion source activated in a vertical borehole is not isotropic and not purely compressional. The confining effects of the borehole on a downhole source are simulated by combining an isotropic explosion (three mutually orthogonal force dipoles with equal strengths) with an additional vertically oriented dipole. This is a specific example of the point tri-dipole source described in section 2.4; the magnitude of the two horizontal dipoles differs from the magnitude of the vertical dipole. Appendix B outlines the procedure for calculating dipole strengths. In this example, the horizontal dipoles are assigned strength 4/3 and the vertical dipole is assigned strength 2/3, relative to the isotropic case in example 2.

Figures 13, 14, and 15 depict velocity, rotation, and pressure traces generated by the tri-dipole source. In order to facilitate comparison with the isotropic explosion source, plot amplitude levels are identical to

figures 10, 11, and 12, respectively. The difference in magnitude between the horizontal and vertical force dipoles is responsible for the shear wave energy radiated from this explosive source.

7.6 Example 4: Unidirectional Torques

Unidirectional point torques oriented in the $+x$, $+y$, and $+z$ directions generate only shear wave arrivals on the particle velocity (figures 16, 17, and 18) and particle rotation (figures 19, 20, and 21) seismograms. Velocity and rotation vector wavefields are orthogonal. The acoustic pressure is identically zero for this pure shear wave source, and thus is not plotted.

7.7 Example 5: Double-Couple With No Net Moment

A small shear dislocation in an elastic medium generates both P-waves and S-waves. This type of source is commonly used to model elastic wavefields produced by microseisms or acoustic emissions, and can be mathematically characterized as a double-couple without moment. In this example, the shear dislocation is represented by orthogonal tension and compression dipoles (equations 2.18a,b). In order to illustrate the complexity of the recorded wavefield amplitudes, dipole orientations taken to be oblique to the coordinates axes. The polar and azimuthal orientation angles for the tension and compression dipoles are $\theta_a = 60°$, $\phi_a = 30°$, and $\theta_b = 150°$, $\phi_b = 30°$, respectively.

Figures 22 and 23 illustrate particle velocity and rotation traces. Although event moveout trajectories are hyperbolae with apexes at the depth of the source, amplitudes are not symmetric or anti-symmetric with respect to the source position. Velocity and rotation wavefields are orthogonal, even though non-zero amplitudes are recorded on all three components of each. Pressure seismograms (figure 24) display similar amplitude asymmetry.

7.8 Example 6: Rotating Horizontal Force

A rotating point force requires some additional explanation. The force density vector of a point force with a time-dependent unit direction vector $\mathbf{a}(t)$ is given by

$$\mathbf{f}(\mathbf{x},t) = Fw(t)\mathbf{a}(t)\delta(\mathbf{x}-\mathbf{x}_s). \tag{7.3}$$

If $\mathbf{a}(t)$ is restricted to a horizontal plane passing through $\mathbf{x}_s$, then it can be expressed as

$$\mathbf{a}(t) = \cos\varphi(t)\,\mathbf{e}_x + \sin\varphi(t)\,\mathbf{e}_y, \tag{7.4}$$

where $\mathbf{e}_x$ and $\mathbf{e}_y$ are unit vectors pointing in the $+x$ and $+y$ directions, respectively. The angle function $\varphi(t)$ describes the orientation of $\mathbf{a}(t)$ in the horizontal plane at time t; the cumulative rotation angle from time $t = 0$ is $\varphi(t) - \varphi(0)$. Combining the above two expressions gives

$$\mathbf{f}(\mathbf{x},t) = Fw(t)\cos\varphi(t)\mathbf{e}_x\delta(\mathbf{x}-\mathbf{x}_s) + Fw(t)\sin\varphi(t)\mathbf{e}_y\delta(\mathbf{x}-\mathbf{x}_s). \tag{7.5}$$

Hence, a rotating point force is represented as a superposition of *two* orthogonal unidirectional point forces. Note, however, that the two source waveforms differ. Each is a trigonometric function modulated by the waveform $w(t)$ of the rotating point force.

Figures 25, 26, and 27 display velocity, rotation, and pressure seismograms produced by a rotating horizontal force. The source waveforms for the x and y components of the applied force are given by the Berlage wavelet (7.1) with the initial phase angle set equal to 0 and $-\pi/2$ radians, respectively. Hence, the rotating waveform $w(t)$ is a positive-going pulse $AH(t)(\omega_0 t)^n \exp(-h\omega_0 t)$, and the rotation period is $T = 1/f_0$. For $f_0 = 80$ Hz, the period equals $T = 12.5$ ms. Careful comparison indicates that figure 25 is *not* merely the sum of the previously computed figures 3 and 4, because the source activation waveforms of the x-component point force (f_x) differ. For the same reason, the rotation traces in figure 26 differ slightly from the sum of figures 6 and 7.

7.9 Example 7: Source Arrays

The final examples indicate that spatially distributed arrays of point sources are easily simulated. The total elastodynamic wavefield radiated from an array is a linear superposition of individual wavefields generated by each point source comprising the array. A basic assumption is that the individual sources are physically non-interacting, i.e., the output of one source does not influence the output of another source.

Figures 28 and 29 depict velocity and rotation seismograms generated by an array of five vertical (f_z) point forces uniformly distributed between depths $z_s = -10$ m and $z_s = +10$ m. Each source is activated with the same Berlage wavform (7.1). P-wave and S-wave arrivals are evident, but moveout trajectories are not exactly hyperbolae. This vertical array clearly enhances horizontally propagating shear wave energy. Destructive interference of the five separate wavefields implies that far-field wavelets have diminished amplitudes and elongated durations at receivers well above/below the source depth (compare with figures 5 and 8). This observation is consistent with a prior theoretical analysis of the elastic waves radiated by a continuous line source of finite length (Aldridge, 1998). The line source acts as a filter that attenuates waves radiated parallel to the source axis, relative to waves radiated perpendicular to the axis.

Array output may be steered in a preferred direction by introducing progressive time shifts into the individual source activation waveforms. Figures 30 and 31 illustrate velocity and rotation seismograms produced by a *focused array* of five non-vertical point forces. As in the previous example, these forces are located between depths $z_s = -10$ m and $z_s = +10$ m, and are separated by a 5 m vertical interval. Geometric focusing of the radiated shear waves onto the receiver at $(x_r, y_r, z_r) = (100, 0, 75)$ m is achieved via two mechanisms:

1) Source activation waveforms are time-shifted Berlage wavelets $w(t-\tau_i)$ for $i = 1 \rightarrow 5$, where individual time shifts are [-6.23, -3.06, 0.00, +2.93, +5.73] ms for sources at [-10, -5, 0, +5, +10] m depth, respectively. These are just the traveltime differences, relative to $z_s = 0$ m, of the shear wave arriving at the distant focal point.

2) Each point force is oriented in the xz plane perpendicular to the line joining the source position and the focal point. Hence, the amplitude of the radiated shear wave is maximized in the direction pointing toward the focal point [see equation (2.5a)].

The figures clearly exhibit strong amplitude enhancement of the shear wave in the vicinity of the receiver at depth $z_r = 75$ m, and amplitude diminution at other depths. However, this constructive/destructive interference is obviously not perfect, due to the extended frequency bandwidth of the source waveforms.

8.0 CONCLUSION

A flexible algorithm has been developed for calculating the elastic wavefield generated by a point source in a homogeneous and isotropic wholespace. The algorithm accommodates a large variety of source and receiver types, deployed in any three-dimensional geometric configuration. Multiple sources and/or receivers may be active simultaneously. Orientations of sources (forces or moments) and directional receivers (velocity or rotation sensors) are unrestricted. Source magnitudes and receiver sensitivities are user-selectable. Synthetic seismic data computed with this algorithm have a variety of uses, including i) testing the validity of elastic responses calculated via purely numerical schemes, ii) testing source parameter inversion algorithms, and iii) designing seismic energy sources or source arrays.

Future improvements to the algorithm may include i) incorporating options for calculating elastic particle displacement and acceleration, and ii) improving the accuracy of the numerical differentiators used to obtain derivatives of the source waveform.

Perhaps the most interesting seismological result obtained from this research is the orthogonality relation between particle velocity and particle rotation wavefields: $(\mathbf{v} \cdot \omega) = 0$. This orthogonality condition holds at all distances and directions from a point source in a homogeneous and isotropic medium. Current generation geophones measure the three components of the particle velocity at the receiver location. Hence, the vector-valued velocity $\mathbf{v}(\mathbf{x}_r, t)$ can be reconstructed. The orthogonality condition implies that the rotation vector at the geophone $\omega(\mathbf{x}_r, t)$ is contained in the time-varying plane perpendicular to $\mathbf{v}(\mathbf{x}_r, t)$. This may provide a clue regarding how to construct a particle rotation sensor, which in turn can be used to isolate the shear portion of a propagating elastodynamic wavefield.

9.0 REFERENCES

Aki, K., and Richards, P.G., 1980, Quantitative seismology, theory and methods, volume 1: W.H. Freeman and Company.

Aldridge, D.F., 1990, The Berlage wavelet: Geophysics, **55**, 1508-1511.

Aldridge, D.F., 1998, Elastic wave radiation from a line source of finite length: Technical report SAND98-2474, Sandia National Laboratories.

Ben-Menahem, A., and Singh, S.J., 1981, Seismic waves and sources: Springer-Verlag.

Eringen, A.C., and Suhubi, E.S., 1975, Elastodynamics, volume 2, linear theory: Academic Press.

Fornberg, B., 1988, Generation of finite difference formulas on arbitrarily spaced grids: Mathematics of Computation, **51**, 699-706.

Graves, R.W., 1996, Simulating seismic wave propagation in 3D elastic media using staggered-grid finite differences: Bulletin of the Seismological Society of America, **86**, 1091-1106.

Heelan, P.A., 1953, Radiation from a cylindrical source of finite length: Geophysics, **18**, 685-696.

Kennett, B.L.N., 1988, Radiation from a moment-tensor source, *in* Seismological Algorithms *edited by* D.J. Doornbos: Academic Press.

Press, W.H., Flannery, B.P., Teukolsky, S.A., and Vetterling, W.T., 1986, Numerical recipes, the art of scientific computing: Cambridge University Press.

Sharpe, J.A., 1942, The production of elastic waves by explosion pressures, I, theory and empirical field observations: Geophysics, **7**, 144-154.

White, J.E., 1983, Underground sound, application of seismic waves: Elsevier.

10.0 APPENDIX A: LOCAL CUBIC POLYNOMIAL APPROXIMATION

The various expressions for velocity, pressure, and rotation require the source waveform $w(t)$ and its first and second derivatives to be evaluated at the P-wave and S-wave retarded times τ_α and τ_β. These times need not coincide with a sample instant t_n of the discretely sampled source waveform $w(t_n)$. In order to obtain values between sample times, the source waveform is locally approximated by a cubic polynomial. Coefficients of the polynomial are determined from four sequential samples of the source function.

Suppose that a cubic polynomial $y(x)$ is fitted to the four equispaced points (x_1, y_1), (x_2, y_2), (x_3, y_3), and (x_4, y_4). The abscissae satisfy $x_{i+1} = x_i + h$ for $i = 1, 2$, and 3. The fitted polynomial and its derivatives are to be evaluated within the middle interval at abscissa $x = x_2 + ph$, where $0 \le p \le 1$. Let the polynomial curve be described by

$$y(x) = y_1 + b(x - x_1) + c(x - x_1)^2 + d(x - x_1)^3, \tag{10.1}$$

and note that $y(x_1) = y_1$ as required. The first and second derivatives of $y(x)$ are

$$y'(x) = b + 2c(x - x_1) + 3d(x - x_1)^2, \tag{10.2}$$

and

$$y''(x) = 2c + 6d(x - x_1), \tag{10.3}$$

respectively. In particular, at $x = x_2 + ph$, then $x - x_1 = h(1+p)$ and thus

$$y(x_2 + ph) = y_1 + bh(1 + p) + ch^2(1 + p)^2 + dh^3(1 + p)^3, \tag{10.4}$$

$$y'(x_2 + ph) = b + 2ch(1 + p) + 3dh^2(1 + p)^2, \tag{10.5}$$

$$y''(x_2 + ph) = 2c + 6dh(1 + p). \tag{10.6}$$

The coefficients b, c, and d in (10.4) through (10.6) are determined by fitting the cubic polynomial to the remaining three points (x_2, y_2), (x_3, y_3), and (x_4, y_4). Hence

$$y(x_2) = y_1 + b(x_2 - x_1) + c(x_2 - x_1)^2 = d(x_2 - x_1)^3 = y_2,$$

or

$$b + ch + dh^2 = \frac{y_2 - y_1}{h}. \tag{10.7a}$$

Similarly, $y(x_3) = y_3$ gives

$$b + 2ch + 4dh^2 = \frac{y_3 - y_1}{2h}, \tag{10.7b}$$

and $y(x_4) = y_4$ gives

$$b + 3ch + 9dh^2 = \frac{y_4 - y_1}{3h}. \tag{10.7c}$$

Organizing equations (10.7a,b,c) into the 3 × 3 linear algebraic system yields

$$\begin{bmatrix} 1 & h & h^2 \\ 1 & 2h & 4h^2 \\ 1 & 3h & 9h^2 \end{bmatrix} \begin{bmatrix} b \\ c \\ d \end{bmatrix} = \frac{1}{h} \begin{bmatrix} (y_2 - y_1)/1 \\ (y_3 - y_1)/2 \\ (y_4 - y_1)/3 \end{bmatrix}. \tag{10.8}$$

The coefficient matrix of (10.8) is a 3 × 3 Vandermonde matrix with determinant $\Delta = 2h^3 \neq 0$. The solution of the system is

$$b = \frac{1}{6h}(-11y_1 + 18y_2 - 9y_3 + 2y_4), \tag{10.9a}$$

$$c = \frac{1}{6h^2}(6y_1 - 15y_2 + 12y_3 - 3y_4), \tag{10.9b}$$

$$d = \frac{1}{6h^3}(-y_1 + 3y_2 - 3y_3 + y_4). \tag{10.9c}$$

Substituting expressions (10.9a,b,c) into (10.4) gives

$$y(x_2 + ph) = a_1 y_1 + a_2 y_2 + a_3 y_3 + a_4 y_4, \tag{10.10}$$

with

$$a_1 = -\frac{1}{6}p(p-1)(p-2), \qquad a_2 = \frac{1}{2}(p+1)(p-1)(p-2), \tag{10.11a,b}$$

$$a_3 = -\frac{1}{2}(p+1)p(p-2), \qquad a_4 = \frac{1}{6}(p+1)p(p-1). \tag{10.11c,d}$$

As a check on the correctness of the derivation, note that the sum of the interpolator coefficients equals unity, as required: $a_1 + a_2 + a_3 + a_4 = 1$. Substituting the solution (10.9) into (10.5) gives

$$y'(x_2 + ph) = \frac{1}{h}(b_1 y_1 + b_2 y_2 + b_3 y_3 + b_4 y_4), \tag{10.12}$$

with

$$b_1 = -\frac{1}{6}(3p^2 - 6p + 2), \qquad b_2 = \frac{1}{2}(3p^2 - 4p - 1), \tag{10.13a,b}$$

$$b_3 = -\frac{1}{2}(3p^2 - 2p - 2), \qquad b_4 = \frac{1}{6}(3p^2 - 1). \tag{10.13c,d}$$

Note that $b_1 + b_2 + b_3 + b_4 = 0$, which is required for differentiator coefficients. Finally, substituting (10.9) into (10.6) yields

$$y''(x_2 + ph) = \frac{1}{h^2}(c_1 y_1 + c_2 y_2 + c_3 y_3 + c_4 y_4), \tag{10.14}$$

where

$$c_1 = 1 - p, \qquad c_2 = 3p - 2, \tag{10.15a,b}$$

$$c_3 = 1 - 3p, \qquad c_4 = p. \tag{10.15c,d}$$

and $c_1 + c_2 + c_3 + c_4 = 0$.

The above formulae are usually used to estimate values of a function $f(x)$ and its first two derivatives at the interior point $x = x_2 + ph$, where $0 \le p \le 1$. In particular, the case $p = 1/2$ yields the familiar centered four-point interpolation and differentiation forms

$$y(x_2 + h/2) = \frac{9}{16}(y_2 + y_3) - \frac{1}{16}(y_1 + y_4) \approx f(x_2 + h/2), \tag{10.16}$$

$$y'(x_2 + h/2) = \frac{1}{h}\left[\frac{9}{8}(y_3 - y_2) - \frac{1}{24}(y_4 - y_1)\right] \approx f'(x_2 + h/2), \tag{10.17}$$

$$y''(x_2 + h/2) = \frac{1}{h^2}\left[-\frac{1}{2}(y_2 + y_3) + \frac{1}{2}(y_1 + y_4)\right] \approx f''(x_2 + h/2). \tag{10.18}$$

Fornberg's (1988) algorithm implies that the centered approximations $y(x_2+h/2)$ and $y'(x_2+h/2)$ possess fourth-order accuracy in the discretization interval h, whereas $y''(x_2+h/2)$ has second-order accuracy. The non-centered approximations (i.e., $p \neq 1/2$) given by equations (10.10), (10.12), and (10.14) have fourth-order, third-order, and second-order accuracy, respectively.

11.0 APPENDIX B: NUMERICAL CALIBRATION OF SOURCE STRENGTH

Calculation of ground motion generated by various seismic energy sources requires knowledge of the source magnitudes. Two explosion seismic sources are considered in this Appendix. An explosion within a spherical cavity generates only outgoing P-wave radiation, whereas an explosion in a small cylindrical cavity radiates both P-waves and S-waves. The latter configuration might represent the confining effects of a borehole on a downhole explosive seismic source (e.g., a borehole airgun). For simplicity, the earth model used in the subsequent analysis is assumed to be a homogeneous and isotropic elastic wholespace with P-wave speed α, S-wave speed β, and mass density ρ.

11.1 Representation of Point Explosions

Algorithms for computing synthetic seismograms usually adopt idealized mathematical representations of seismic energy sources as a combination of one or more point forces, dipoles, couples, etc. The strengths or magnitudes of these point sources are required to compute ground motion in physical units.

A point source of compression (i.e., an explosion) can be represented by three mutually orthogonal force dipoles of equal strength M_c. The scalar M_c has dimension "moment" (force times distance, or energy). The far-field particle velocity vector radiated by this source in a homogeneous and isotropic elastic wholespace is

$$\mathbf{v}_c\big|_{\text{far}} = \frac{M_c}{4\pi\rho}\left[\frac{w''(\tau_\alpha)}{\alpha^3 R}\right]\mathbf{e}_R, \tag{11.1}$$

where R is the source-receiver distance, $\mathbf{e}_R$ is a unit vector pointing from source to receiver, $w(t)$ is a (dimensionless) source waveform, and $\tau_\alpha = t - R/\alpha$ is the P-wave retarded time. The far-field velocity consists of compressional waves polarized in the propagation direction $\mathbf{e}_R$; the velocity waveform is the second derivative of the source moment wavelet $w(t)$.

Suppose that the point source of compression is combined with a vertically oriented force dipole with moment strength M_d. The far-field velocity generated by the dipole is

$$\mathbf{v}_d\big|_{\text{far}} = \frac{M_d}{4\pi\rho}\left[\frac{\cos^2\theta\, w''(\tau_\alpha)}{\alpha^3 R}\mathbf{e}_R - \frac{\sin\theta\cos\theta\, w''(\tau_\beta)}{\beta^3 R}\mathbf{e}_\theta\right], \tag{11.2}$$

where the polar angle θ is measured from the $+z$ axis in a spherical coordinate system centered at the source location. The corresponding unit vector is $\mathbf{e}_\theta$. Also, $\tau_\beta = t - R/\beta$ is the S-wave retarded time. The dipole source radiates both longitudinal P-waves and transverse S-waves to the far-field; the waveform of each is given by the second derivative of the source wavelet. Adding the above two expressions gives the far-field velocity vector generated by the combined point source of compression and vertical force dipole:

$$\mathbf{v}_{c+d}\big|_{\text{far}} = \mathbf{v}_c\big|_{\text{far}} + \mathbf{v}_d\big|_{\text{far}} = \frac{M_c}{4\pi\rho}\left[\frac{w''(\tau_\alpha)}{\alpha^3 R}\right]\mathbf{e}_R + \frac{M_d}{4\pi\rho}\left[\frac{\cos^2\theta\, w''(\tau_\alpha)}{\alpha^3 R}\mathbf{e}_R - \frac{\sin\theta\cos\theta\, w''(\tau_\beta)}{\beta^3 R}\mathbf{e}_\theta\right]. \tag{11.3}$$

This source is represented by three mutually perpendicular dipoles with unequal magnitudes. The strength of the two horizontally oriented dipoles is $M_{hor} = M_c$, while the strength of the vertical dipole is $M_{ver} = M_c + M_d$.

11.2 Explosion Source Strength Calibration

Numerical values of the moment scalars M_c, M_{hor}, and M_{ver} are required in a synthetic seismogram computation algorithm. These are determined by comparing the above expressions for far-field particle velocity with expressions for the velocity vector generated by explosions within simply shaped cavities.

Consider a small spherical cavity of radius a located in a homogeneous and isotropic elastic wholespace. If a time-varying pressure $p(t) = p_0 w(t)$ is applied to the cavity wall, then radially polarized compressional waves are generated that propagate away from the cavity with the P-wave speed α. As $p_0 \to \infty$ and $v_0 = (4/3)\pi a^3 \to 0$ such that $E_0 = p_0 v_0$ remains finite, then a point spherical cavity source is obtained. E_0 is a pressure-volume product characterizing the strength of the source; note that E_0 has physical dimension of energy. From Sharpe (1944), the far-field particle velocity radiated by this source is

$$\mathbf{v}_{sphere}\big|_{far} = \frac{(3/4)(\alpha/\beta)^2 E_0}{4\pi\rho}\left[\frac{w''(\tau_\alpha)}{\alpha^3 R}\right]\mathbf{e}_R . \tag{11.4}$$

This equation has the *same* mathematical form as the velocity generated by the point source of compression represented by three orthogonal force dipoles [equation (11.1) above]. Comparing the two expressions indicates that the dipole strengths should be assigned as

$$M_c = \frac{3}{4}(\alpha/\beta)^2 E_0 . \tag{11.5}$$

Example:

For $v_0 = 6.55 \times 10^{-4}$ m^3 and $p_0 = 2.07 \times 10^7$ P (corresponding to $v_0 = 40$ in^3 and $p_0 = 3000$ psi) the pressure-volume product evaluates to $E_0 = 1.36 \times 10^4$ J. Assuming $\alpha/\beta = 2$, then the moment magnitude is approximately $M_c = 4.08 \times 10^4$ N-m. At radial distance $R = 100$ m in an elastic medium with P-wave speed $\alpha = 2000$ m/s and mass density $\rho = 2000$ kg/m^2, this explosive source would produce a maximum particle velocity of $v_{max} = (2.03 \times 10^{-12}$ m-s) max $|w''(t)|$, where the latter symbol stands for the maximum absolute value of the second derivative of the source wavelet (SI units: s^{-2}). If the source waveform is a sinusoidal function with frequency f_0, then max $|w''(t)| = (2\pi f_0)^2$, and the maximum particle velocity becomes $v_{max} = 8.01 \times 10^{-11} f_0^2$ m/s.

Now consider a small cylindrical cavity of radius a and length h, with axis parallel to the z-axis of the coordinate system. The circular walls of the cavity (but *not* the end caps) are subject to the pressure $p(t) = p_0 w(t)$. In the limit as $p_0 \to \infty$ and $v_0 = \pi a^2 h \to 0$ such that the pressure-volume product $E_0 = p_0 v_0$ remains finite, the far-field velocity vector generated by this source is

$$\mathbf{v}_{cylinder}\big|_{far} = \frac{(\alpha/\beta)^2 E_0}{4\pi\rho}\left[\frac{w''(\tau_\alpha)}{\alpha^3 R}\right]\mathbf{e}_R + \frac{-2E_0}{4\pi\rho}\left[\frac{\cos^2\theta\, w''(\tau_\alpha)}{\alpha^3 R}\mathbf{e}_R - \frac{\sin\theta\cos\theta\, w''(\tau_\beta)}{\beta^3 R}\mathbf{e}_\theta\right], \tag{11.6}$$

(Heelan, 1953). The pressurized cylindrical cavity radiates both longitudinal P-waves and transverse S-waves to the far-field. The above equation has the same structure as the velocity generated by the point source of compression plus vertical dipole [equation (11.3) above]. Comparing the two expressions indicates that the horizontal and vertical force dipoles of the latter should be assigned magnitudes

$$M_{hor} = (\alpha/\beta)^2 E_0, \qquad M_{ver} = [(\alpha/\beta)^2 - 2]E_0. \tag{11.7a,b}$$

Assuming that the pressure-volume product E_0 for the point source of compression is identical, then relative to the moment strength M_c these dipole strengths are

$$\frac{M_{hor}}{M_c} = \frac{4}{3}, \qquad \frac{M_{ver}}{M_c} = \frac{4}{3}\left[1 - 2(\beta/\alpha)^2\right]. \tag{11.8a,b}$$

In the case of earth materials where β/α = 1/2 the ratio M_{ver}/M_c = 2/3. This difference in magnitude between M_{ver} and M_{hor} is responsible for the shear wave energy radiated from an explosive source in a small cylindrical cavity.

12.0 FIGURES

Figure 1: Source wavelet $w(t)$ and its first and second derivatives. Each waveform is normalized to unit maximum absolute amplitude. The source pulse is a Berlage wavelet with main frequency f_0 = 80 Hz, damping factor h = 1.0, time exponent n = 3, and initial phase angle θ_0 = -90°.

Figure 2: Frequency amplitude spectra of the source wavelet and its first and second derivatives. Each spectrum is normalized to unit maximum amplitude. Peak amplitude spectrum values occur at 82.0 Hz, 97.7 Hz, and 113.3 Hz for $w(t)$, $w'(t)$, and $w''(t)$, respectively.

Figure 3: Three-component particle velocity seismograms generated by a horizontal point force oriented in the $+x$ direction.

Figure 4: Three-component particle velocity seismograms generated by a horizontal point force oriented in the $+y$ direction.

Figure 5: Three-component particle velocity seismograms generated by a vertical point force oriented in the $+z$ direction.

Figure 6: Three-component particle rotation seismograms generated by a horizontal point force oriented in the $+x$ direction.

Figure 7: Three-component particle rotation seismograms generated by a horizontal point force oriented in the $+y$ direction.

Figure 8: Three-component particle rotation seismograms generated by a vertical point force oriented in the $+z$ direction.

Figure 9: Acoustic pressure seismograms generated by point forces oriented in the $+x$, $+y$, and $+z$ directions.

Figure 10: Three-component particle velocity seismograms generated by an isotropic point explosion.

Figure 11: Three-component particle rotation seismograms generated by an isotropic point explosion. All traces are identically zero.

Figure 12: Acoustic pressure seismograms generated by an isotropic point explosion.

Figure 13: Three-component particle velocity seismograms generated by a point source of compression combined with a vertically oriented force dipole.

Figure 14: Three-component particle rotation seismograms generated by a point source of compression combined with a vertically oriented force dipole.

Figure 15: Pressure seismograms generated by a point source of compression combined with a vertically oriented force dipole.

Figure 16: Three-component particle velocity seismograms generated by a point torque oriented in the $+x$-direction.

Figure 17: Three-component particle velocity seismograms generated by a point torque oriented in the $+y$-direction.

Figure 18: Three-component particle velocity seismograms generated by a point torque oriented in the $+z$-direction.

Figure 19: Three-component particle rotation seismograms generated by a point torque oriented in the $+x$-direction.

Figure 20: Three-component particle rotation seismograms generated by a point torque oriented in the $+y$-direction.

Figure 21: Three-component particle rotation seismograms generated by a point torque oriented in the $+z$-direction.

Figure 22: Three-component particle velocity seismograms generated by a point double-couple without moment.

Figure 23: Three-component particle rotation seismograms generated by a point double-couple without moment.

Figure 24: Acoustic pressure seismograms generated by a point double-couple without moment.

Figure 25: Three-component particle velocity seismograms generated by a rotating horizontal point force.

Figure 26: Three-component particle rotation seismograms generated by a rotating horizontal point force.

Figure 27: Acoustic pressure seismograms generated by a rotating horizontal point force.

Figure 28: Three-component particle velocity seismograms generated by a distributed array of five vertical point forces.

Figure 29: Three-component particle rotation seismograms generated by a distributed array of five vertical point forces.

Figure 30: Three-component particle velocity seismograms generated by a focused array of five non-vertical point forces. Focal point is at receiver at depth $z_r = +75$ m.

Figure 31: Three-component particle rotation seismograms generated by a focused array of five non-vertical point forces. Focal point is at receiver at depth $z_r = +75$ m.

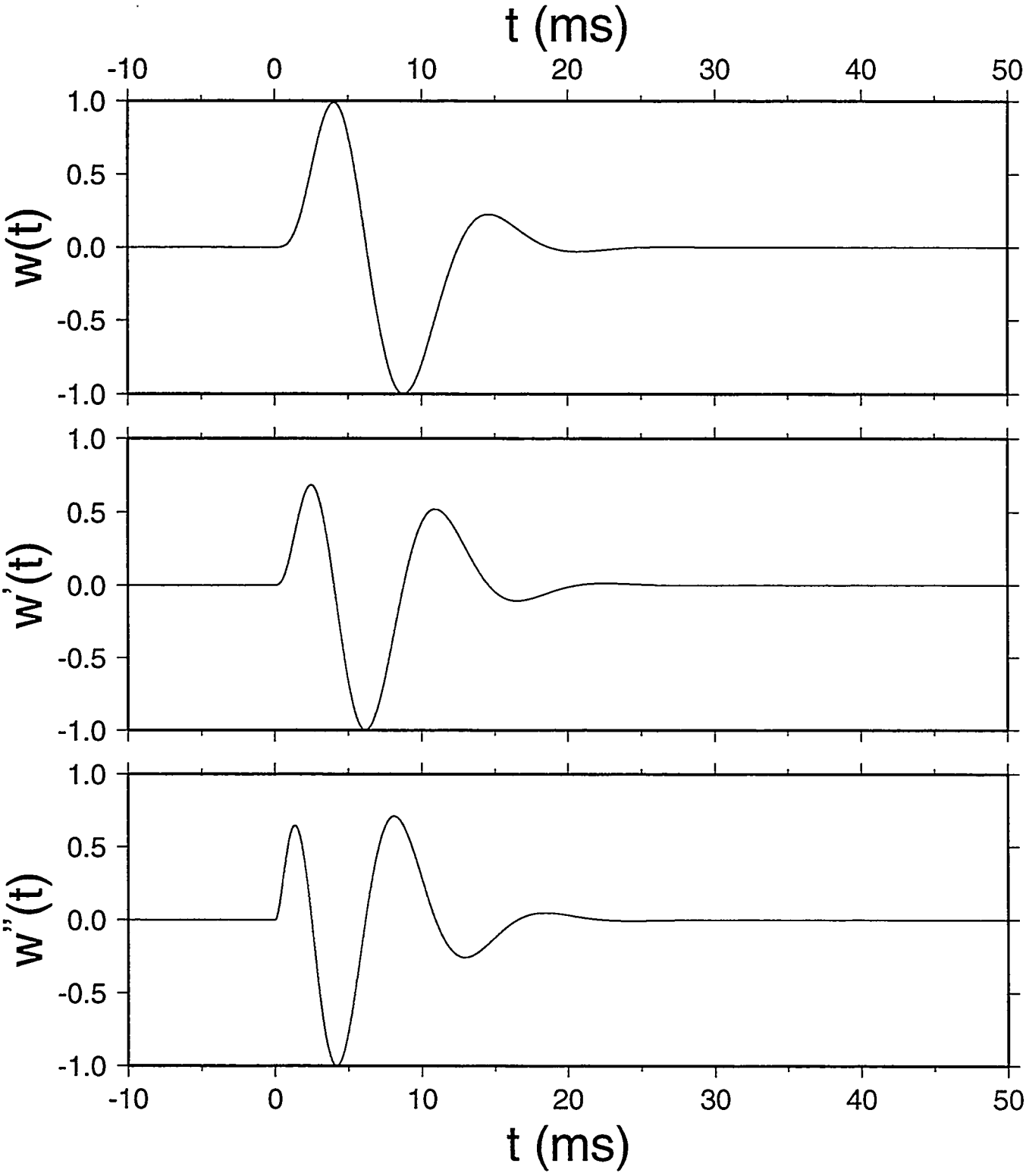

Figure 1

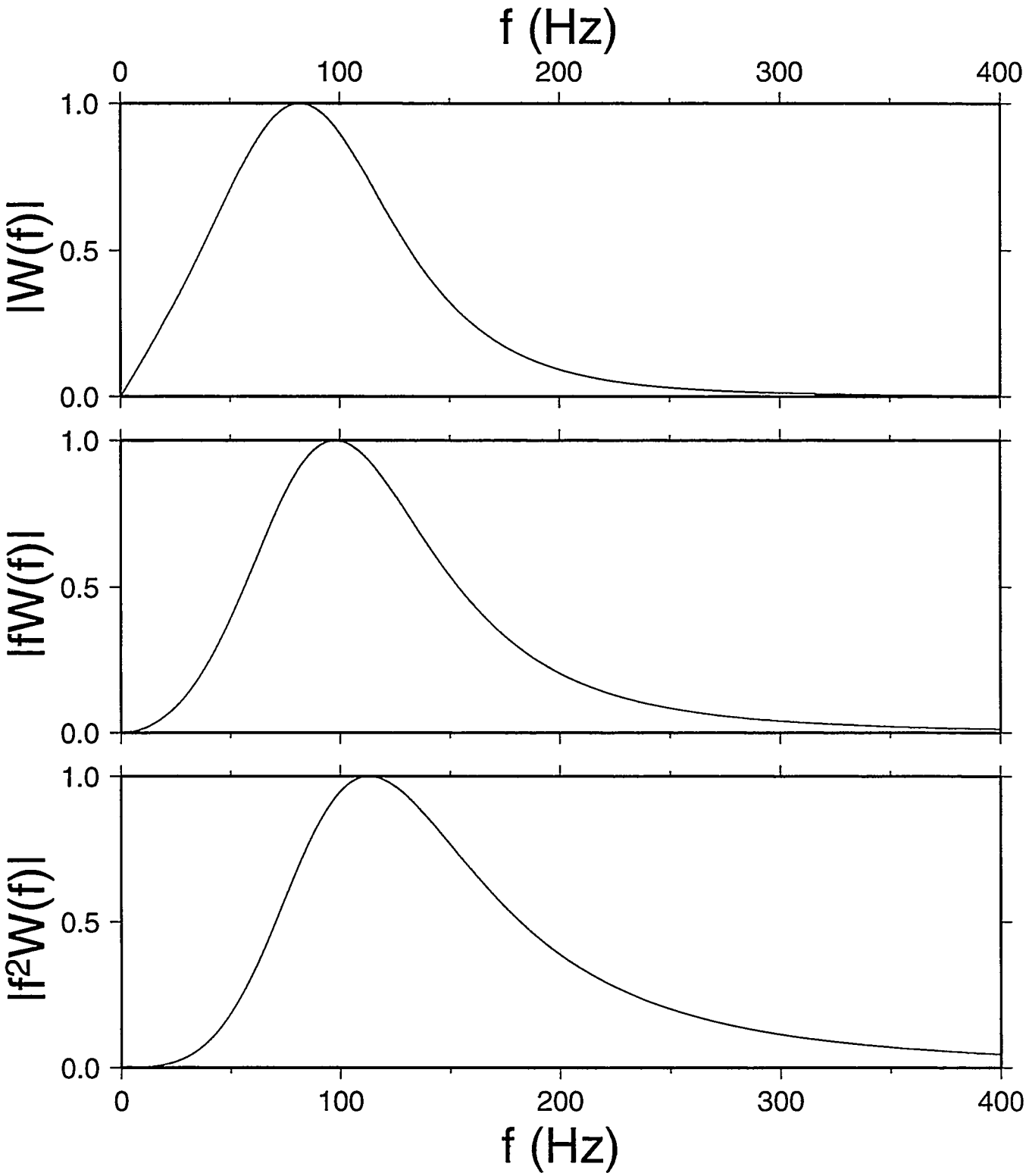

Figure 2

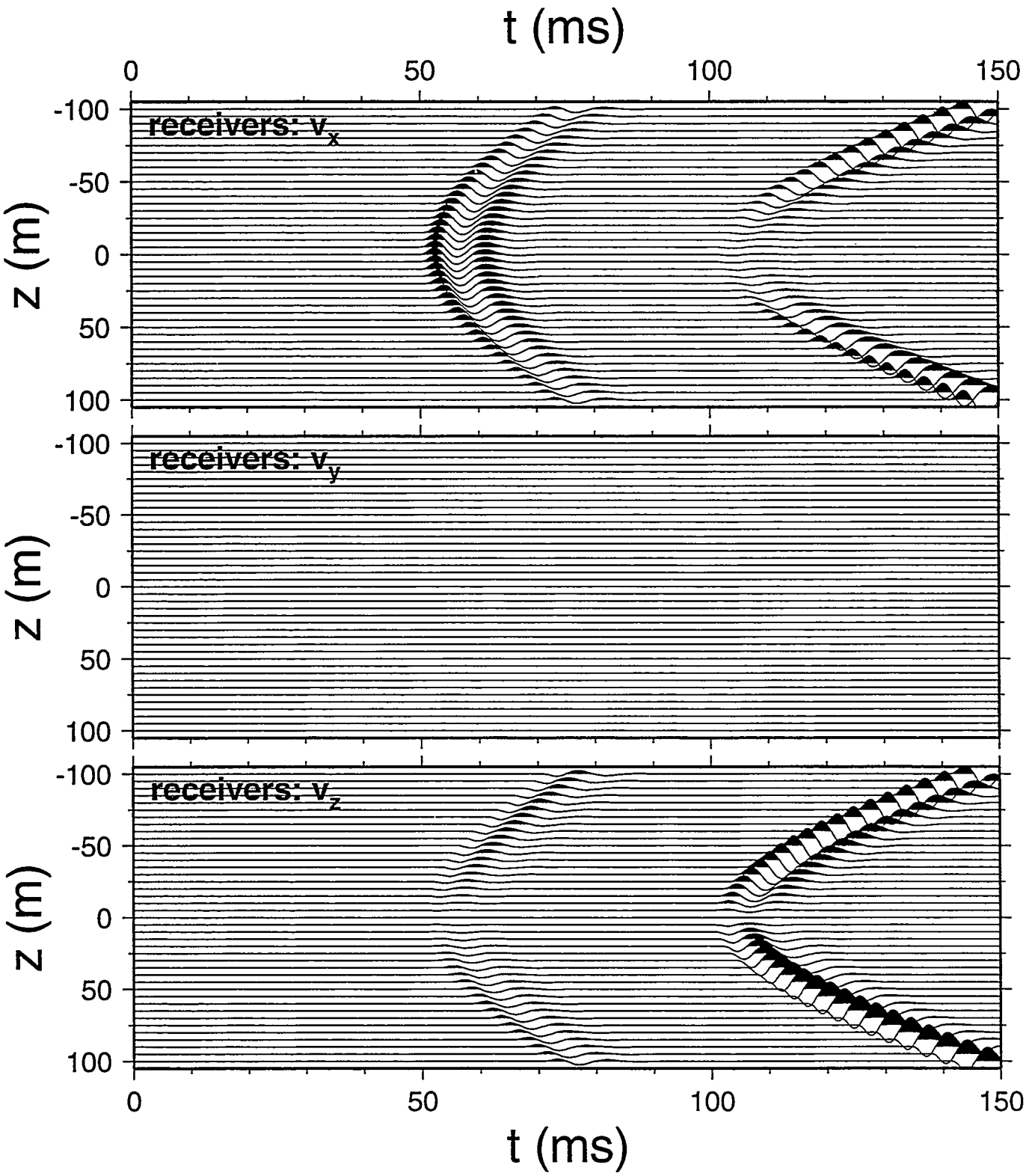

Figure 3 **Source: fx force**

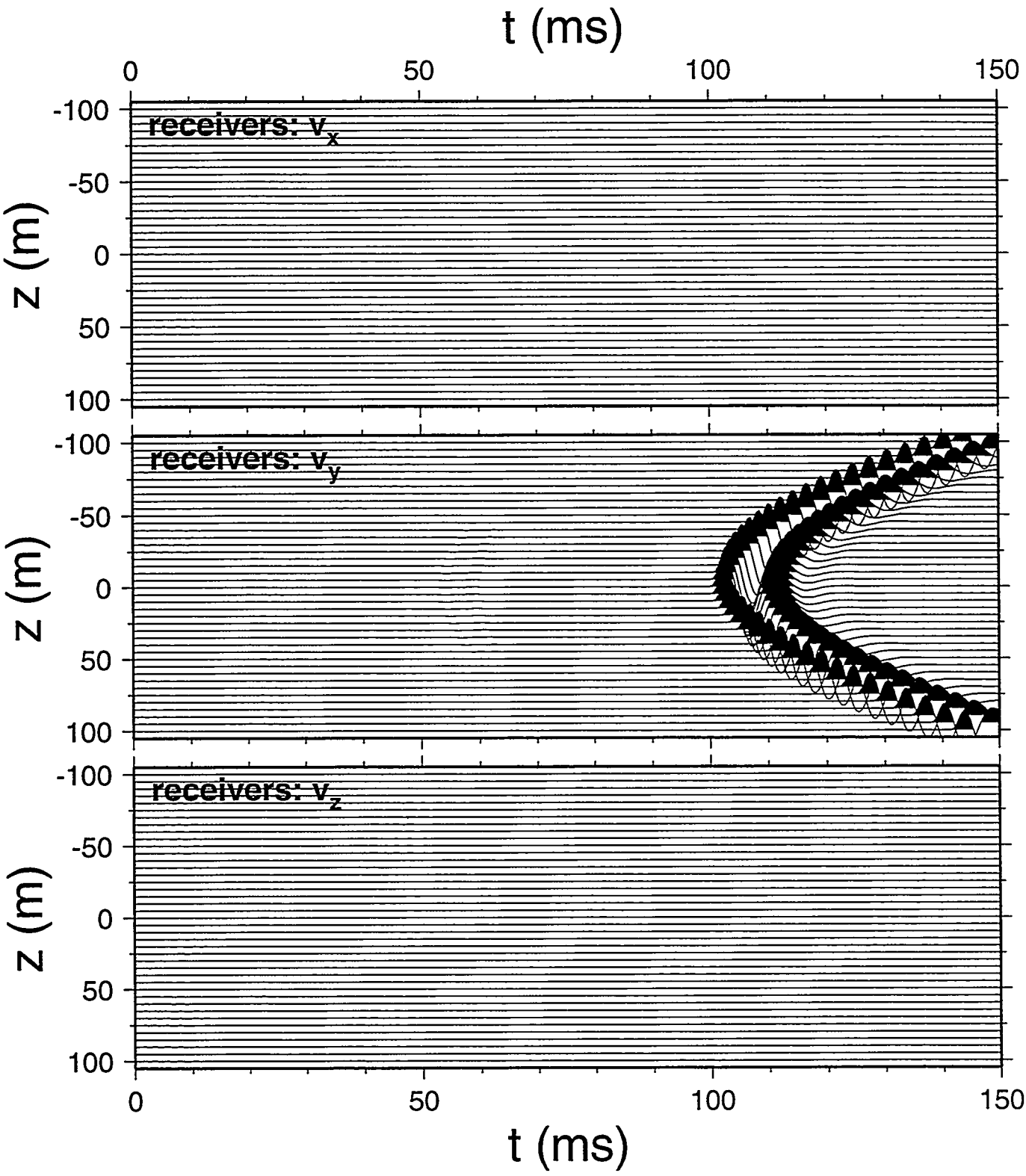

Figure 4 **Source: fy force**

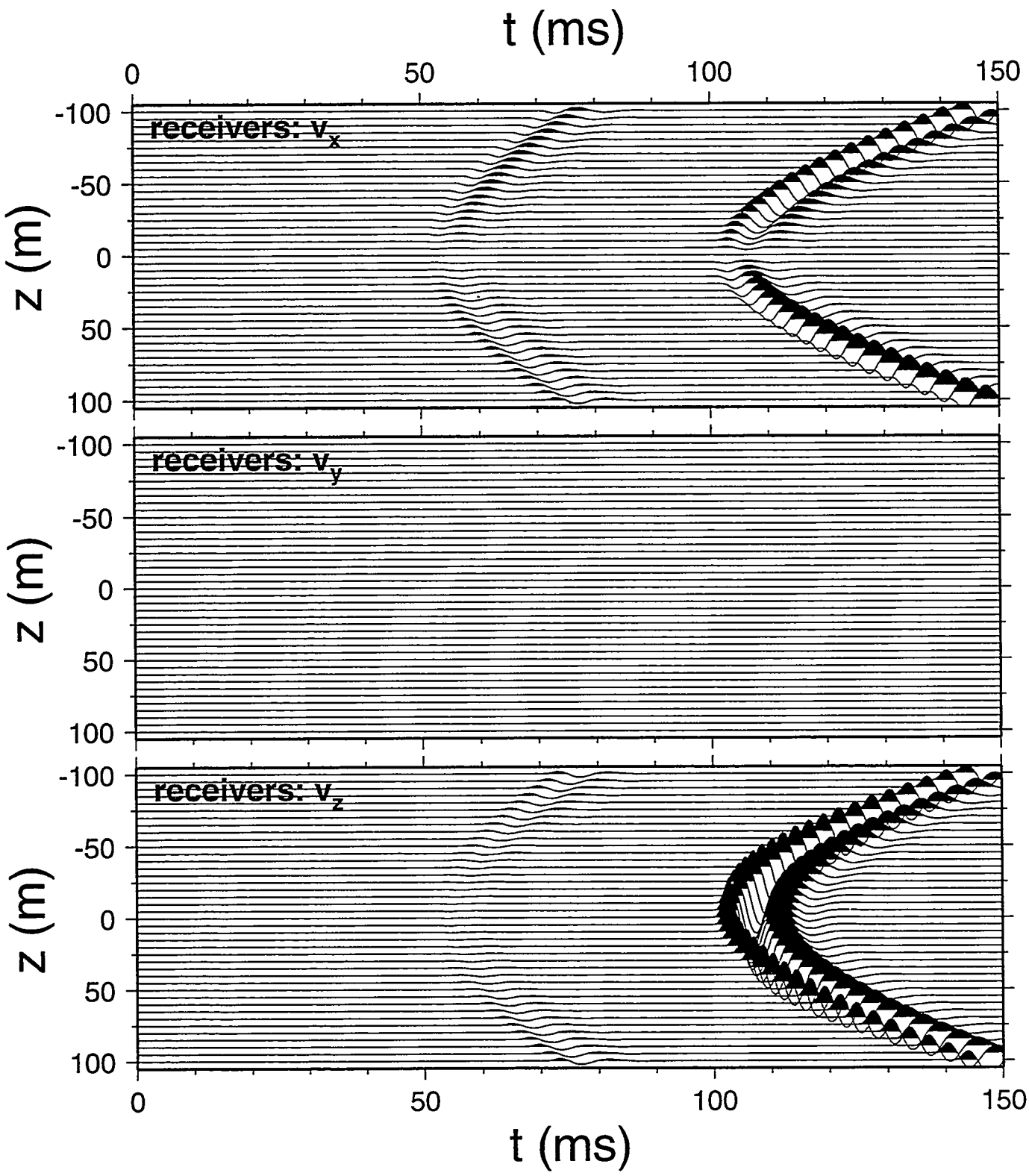

Figure 5 **Source: fz force**

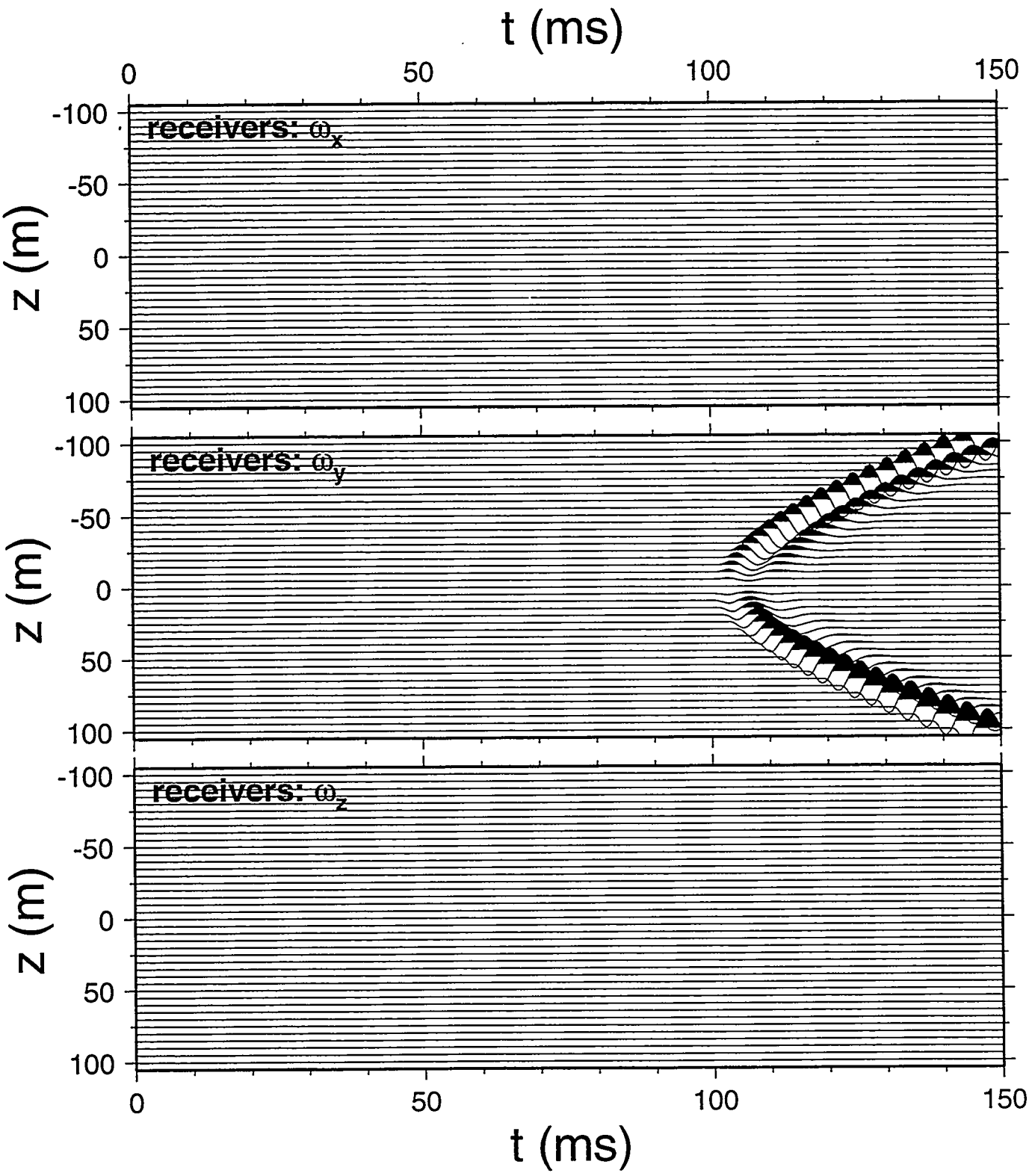

Figure 6 **Source: fx force**

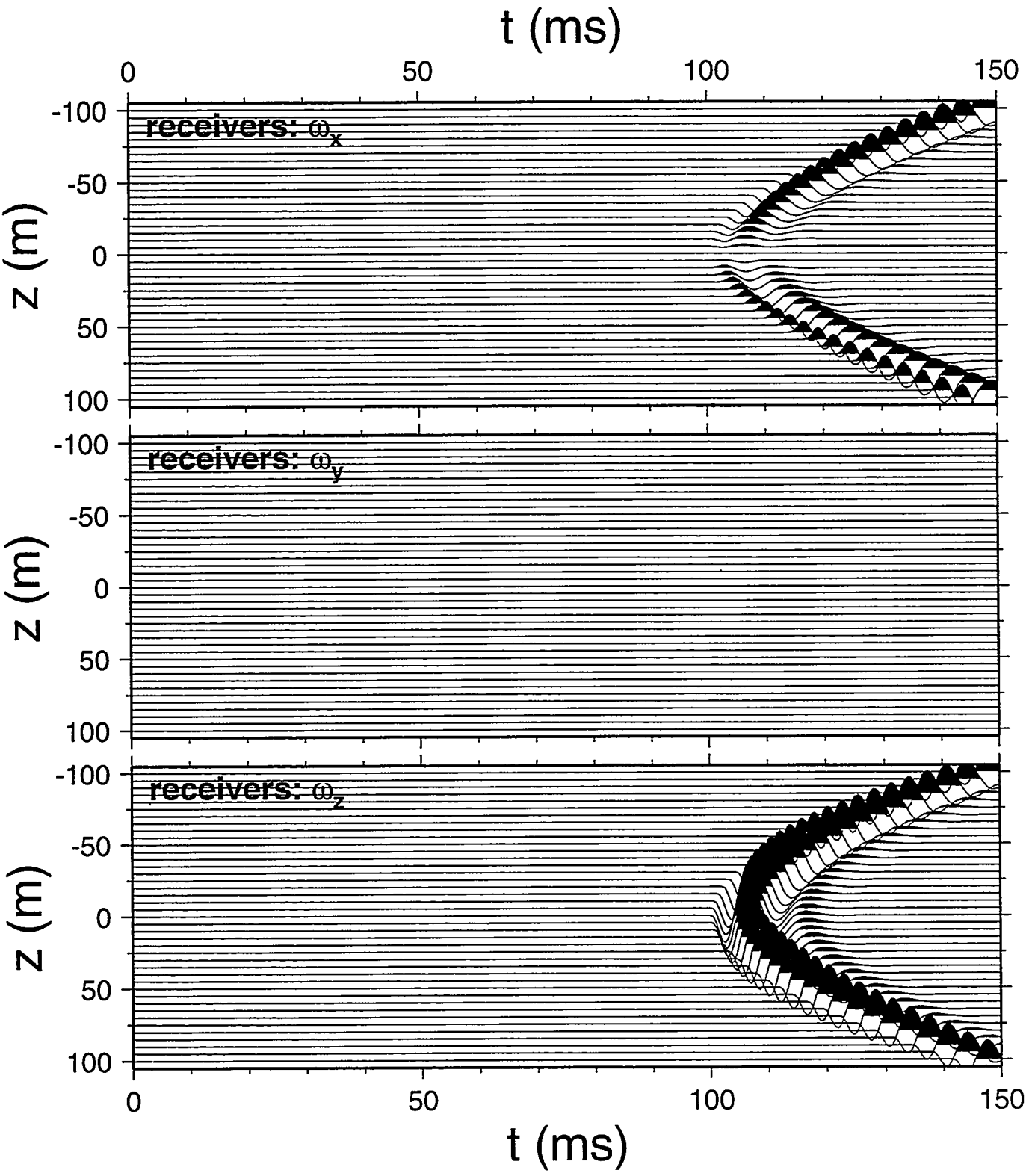

Figure 7 **Source: fy force**

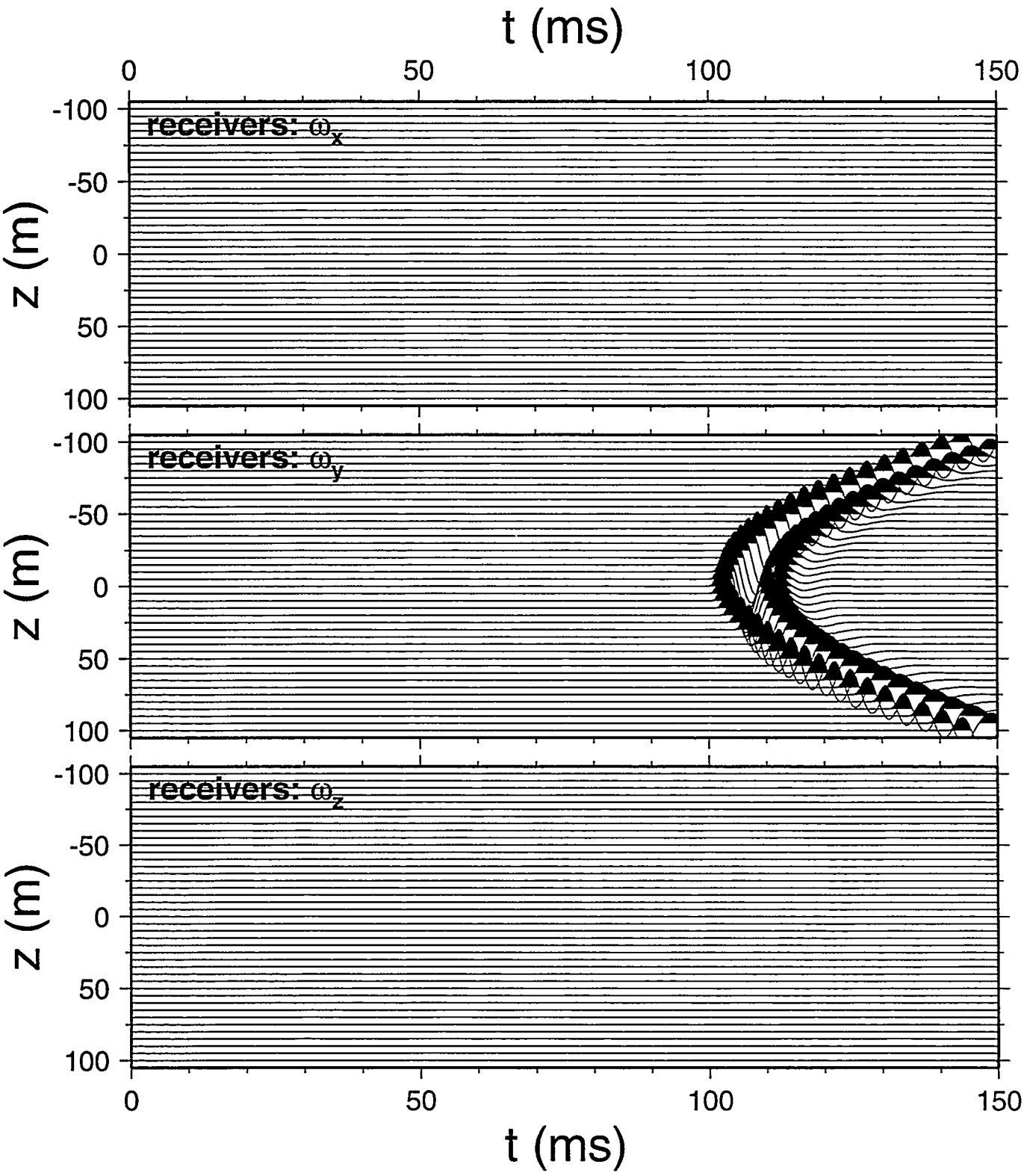

Figure 8 **Source: fz force**

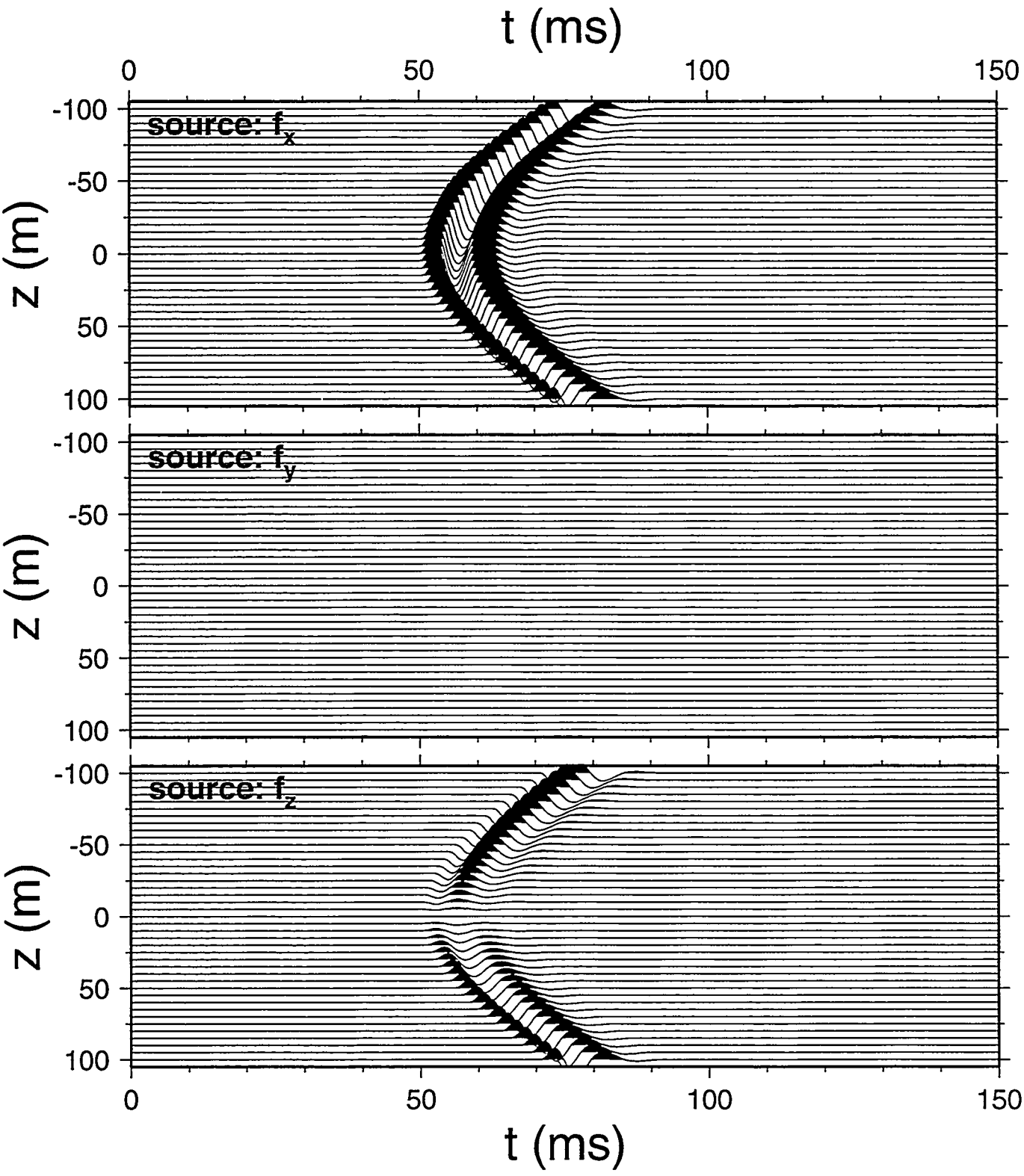

Figure 9 **Receivers: p**

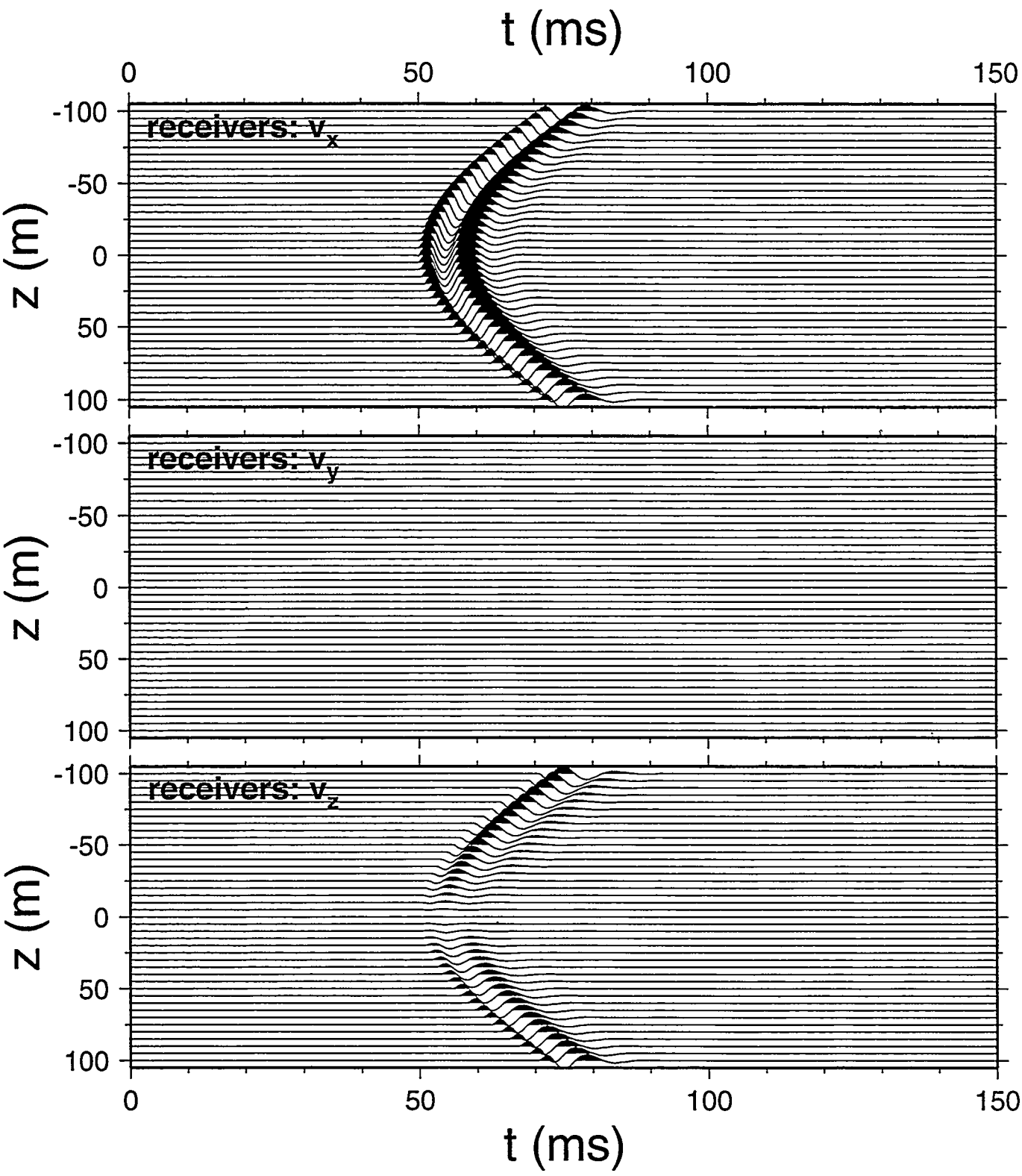

Figure 10 **Source: explosion**

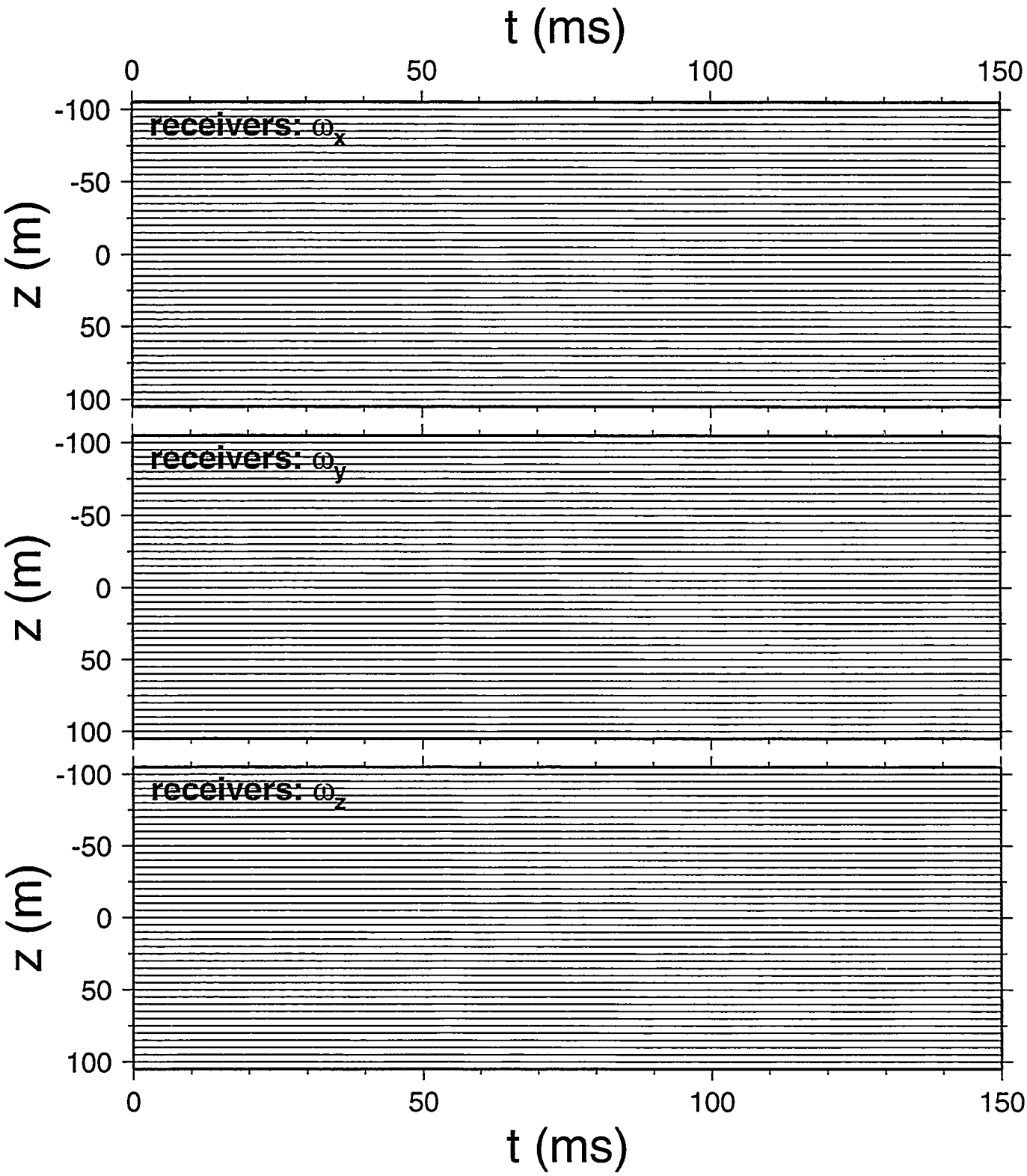

Figure 11 **Source: explosion**

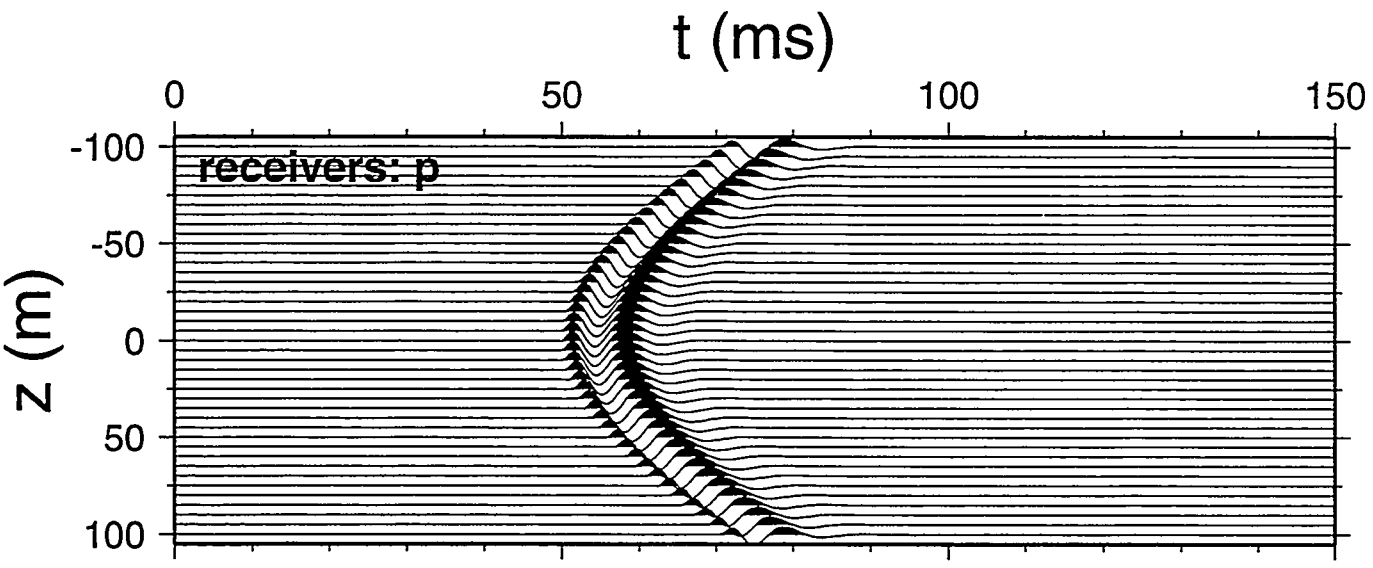

Figure 12 **Source: explosion**

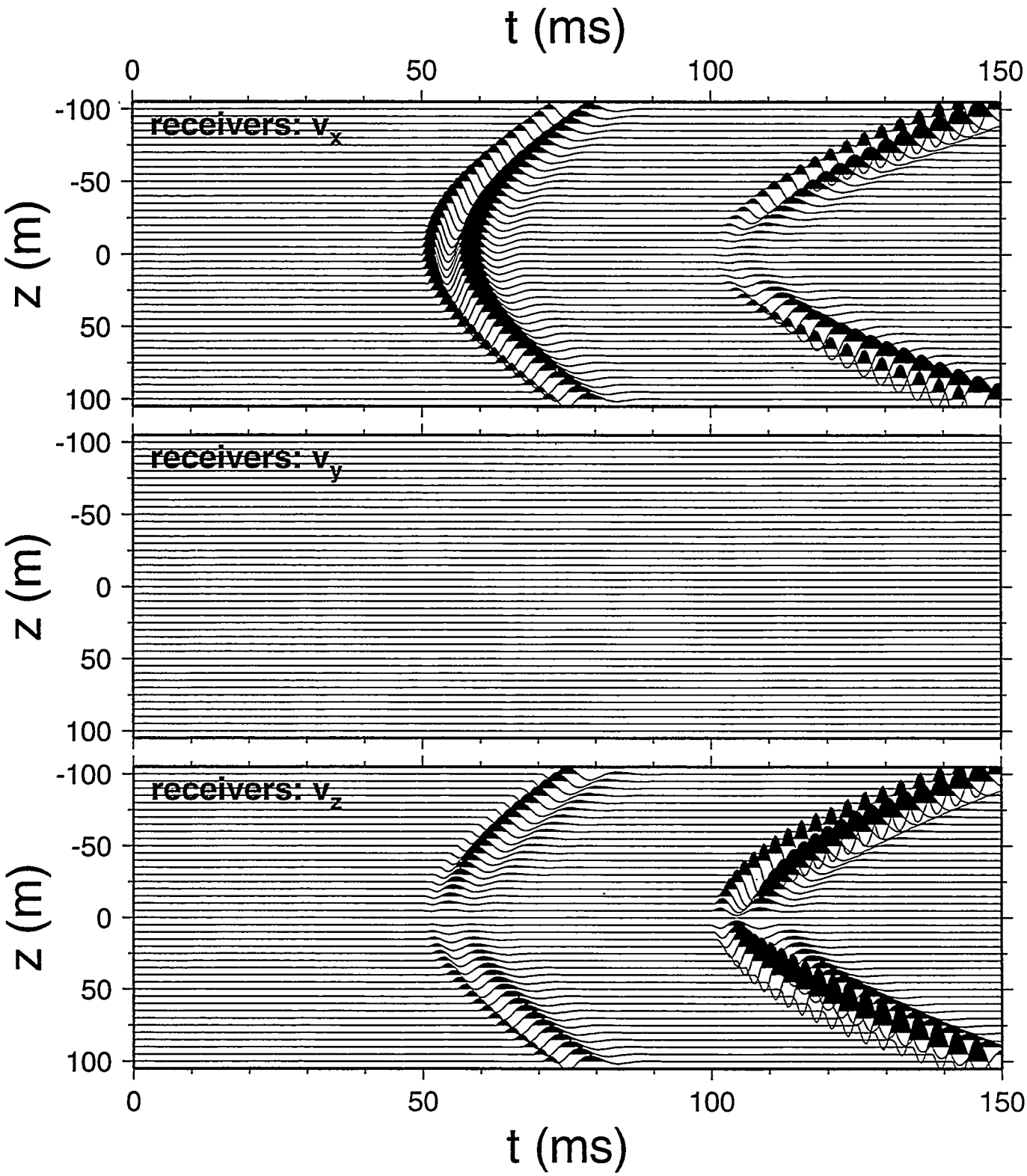

Figure 13

Source: explosion + vertical dipole

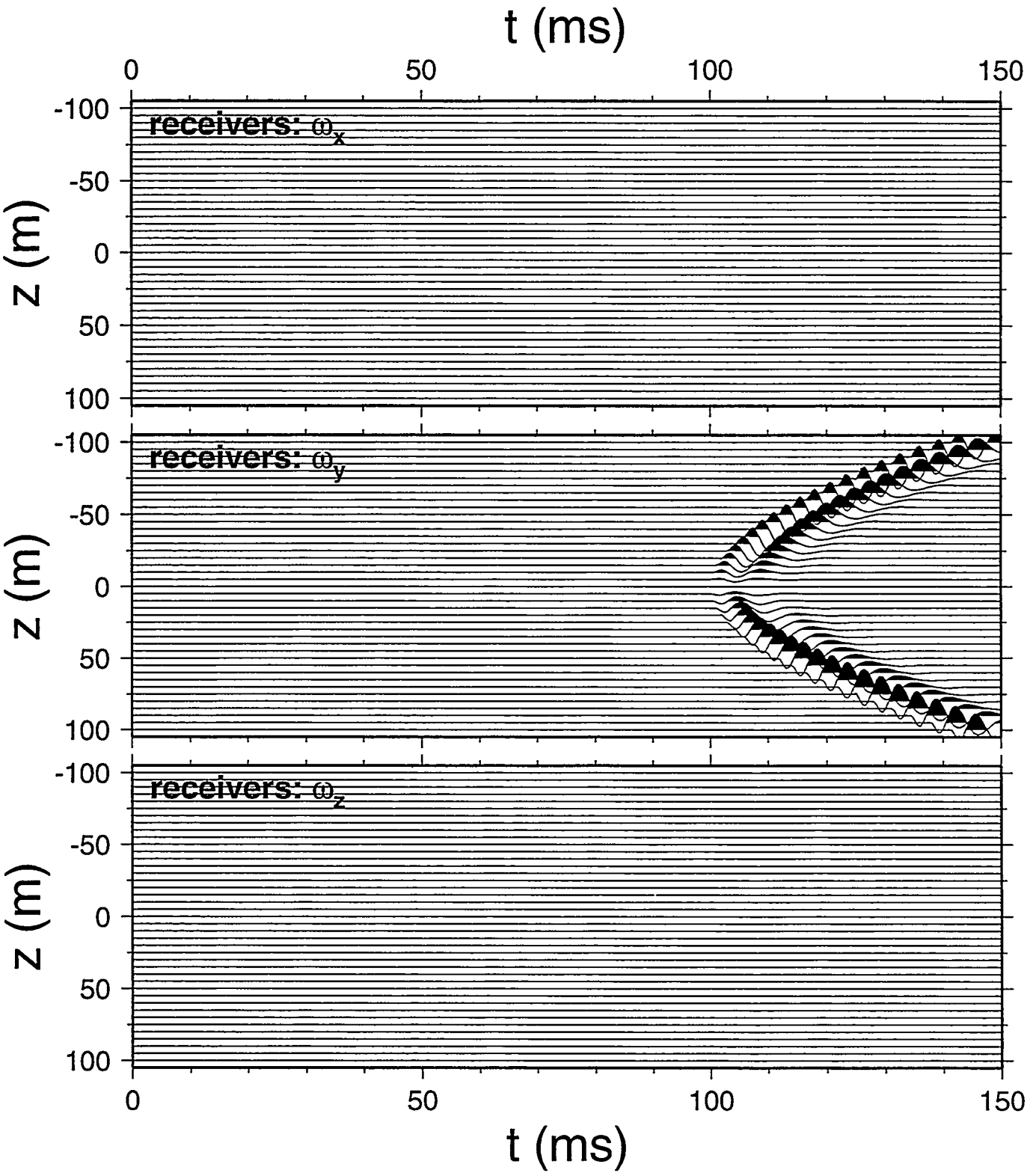

Figure 14

Source: explosion + vertical dipole

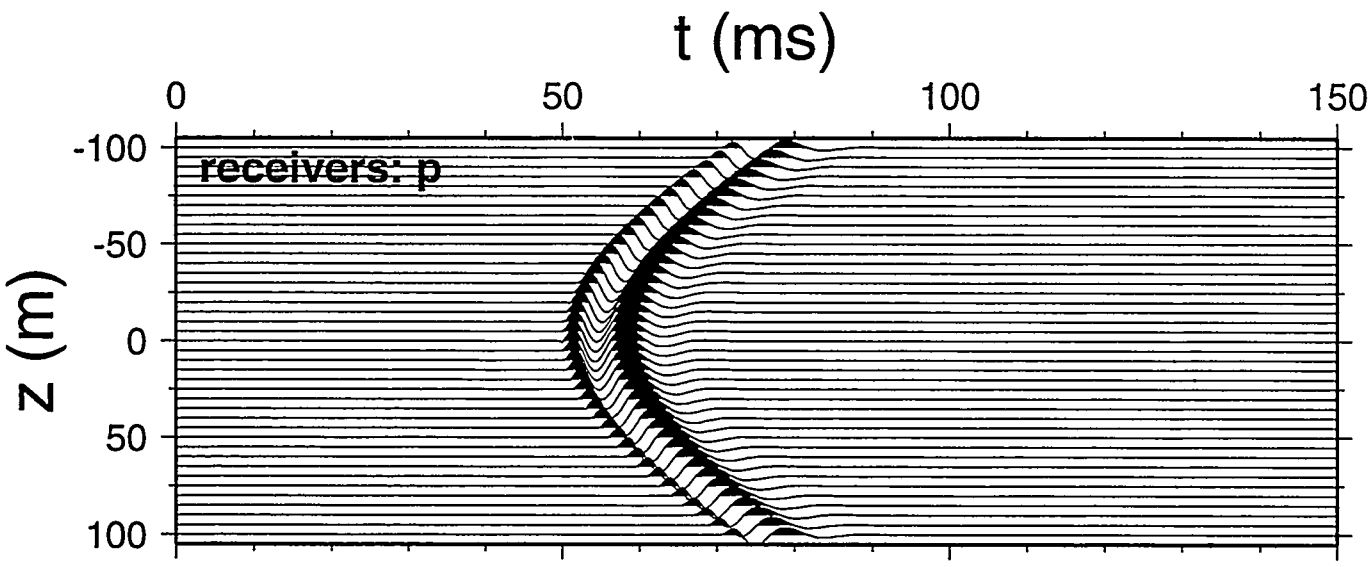

Figure 15

Source: explosion + vertical dipole

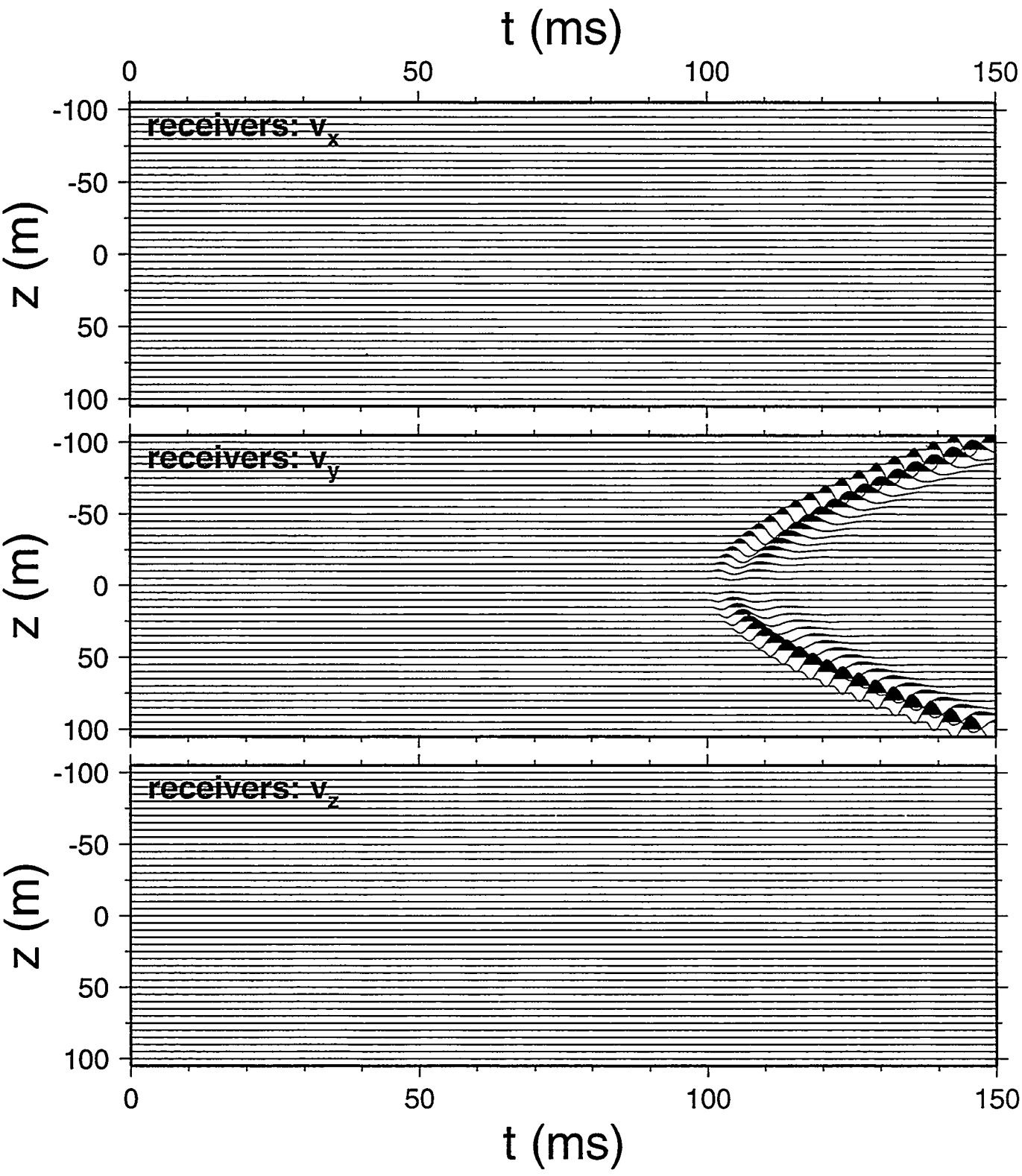

Figure 16 **Source: tx torque**

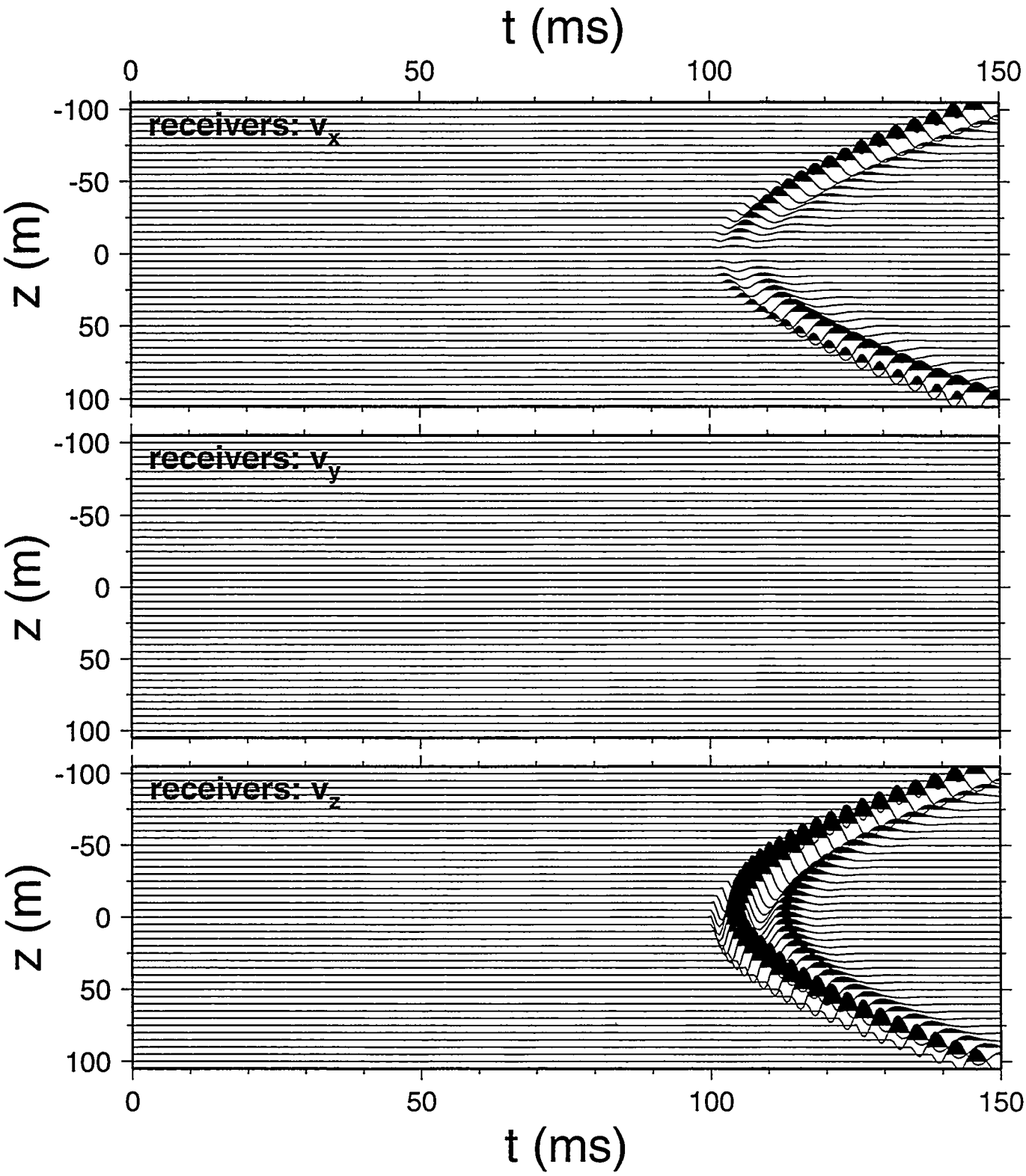

Figure 17 **Source: ty torque**

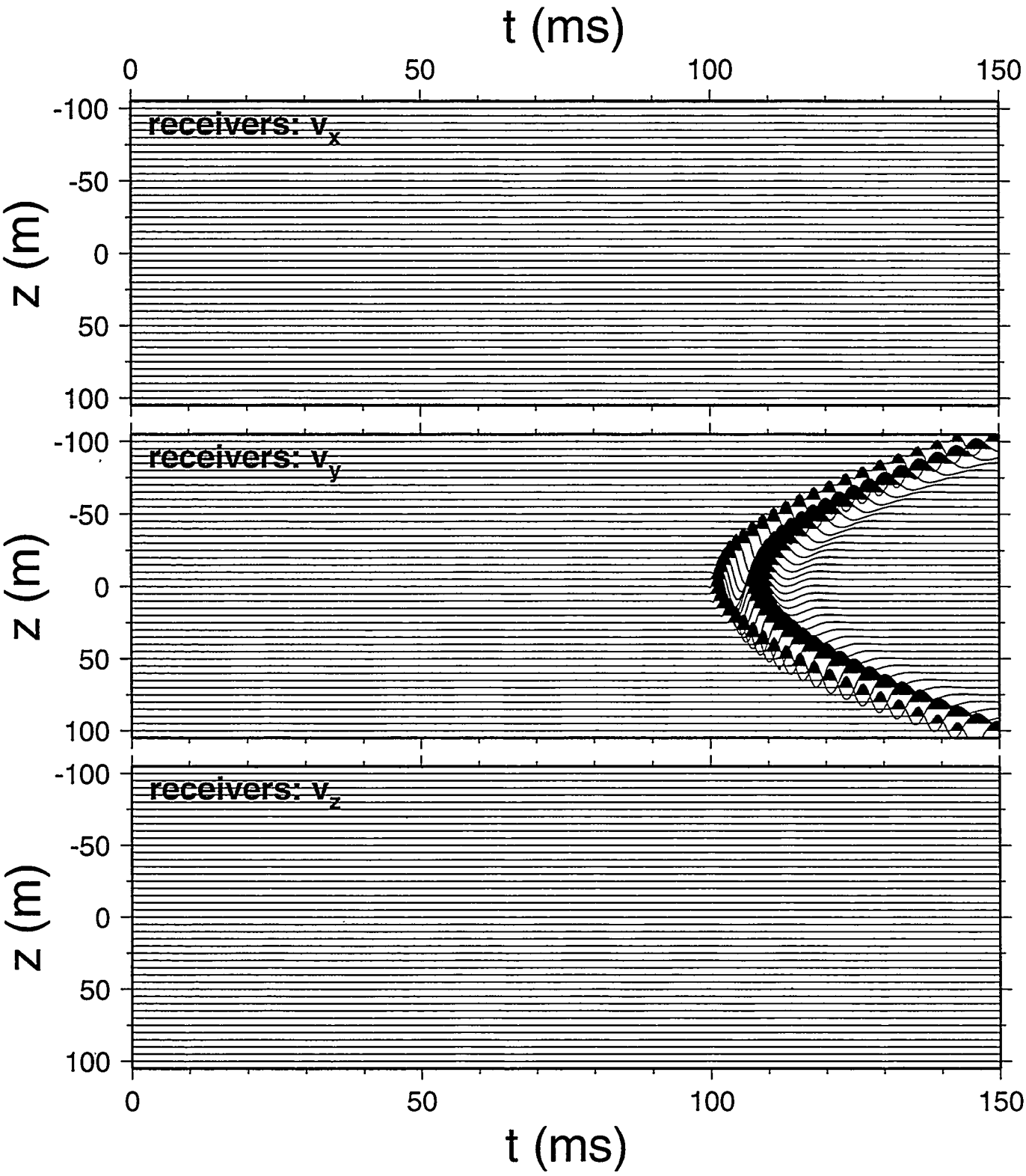

Figure 18 **Source: tz torque**

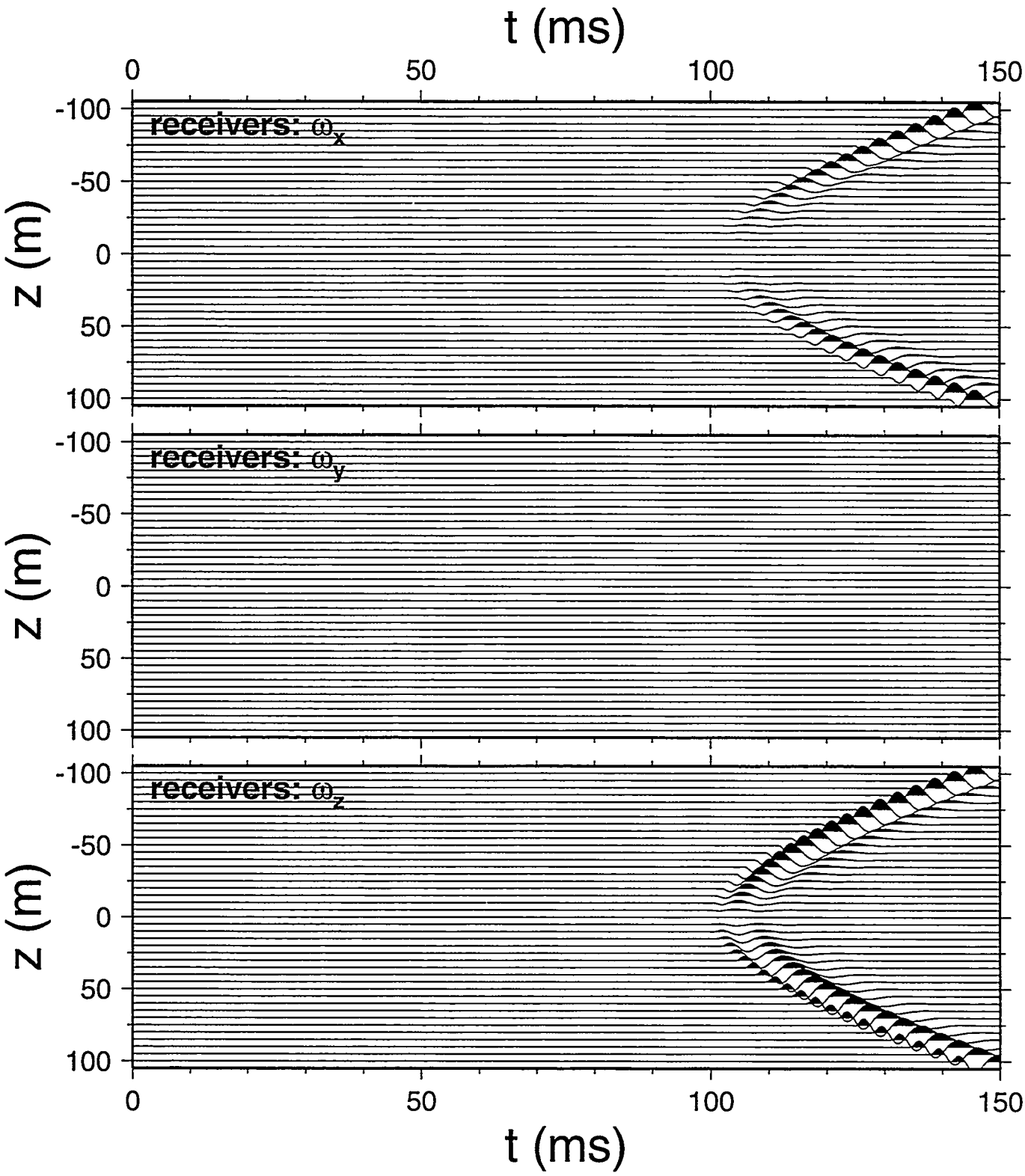

Figure 19 **Source: tx torque**

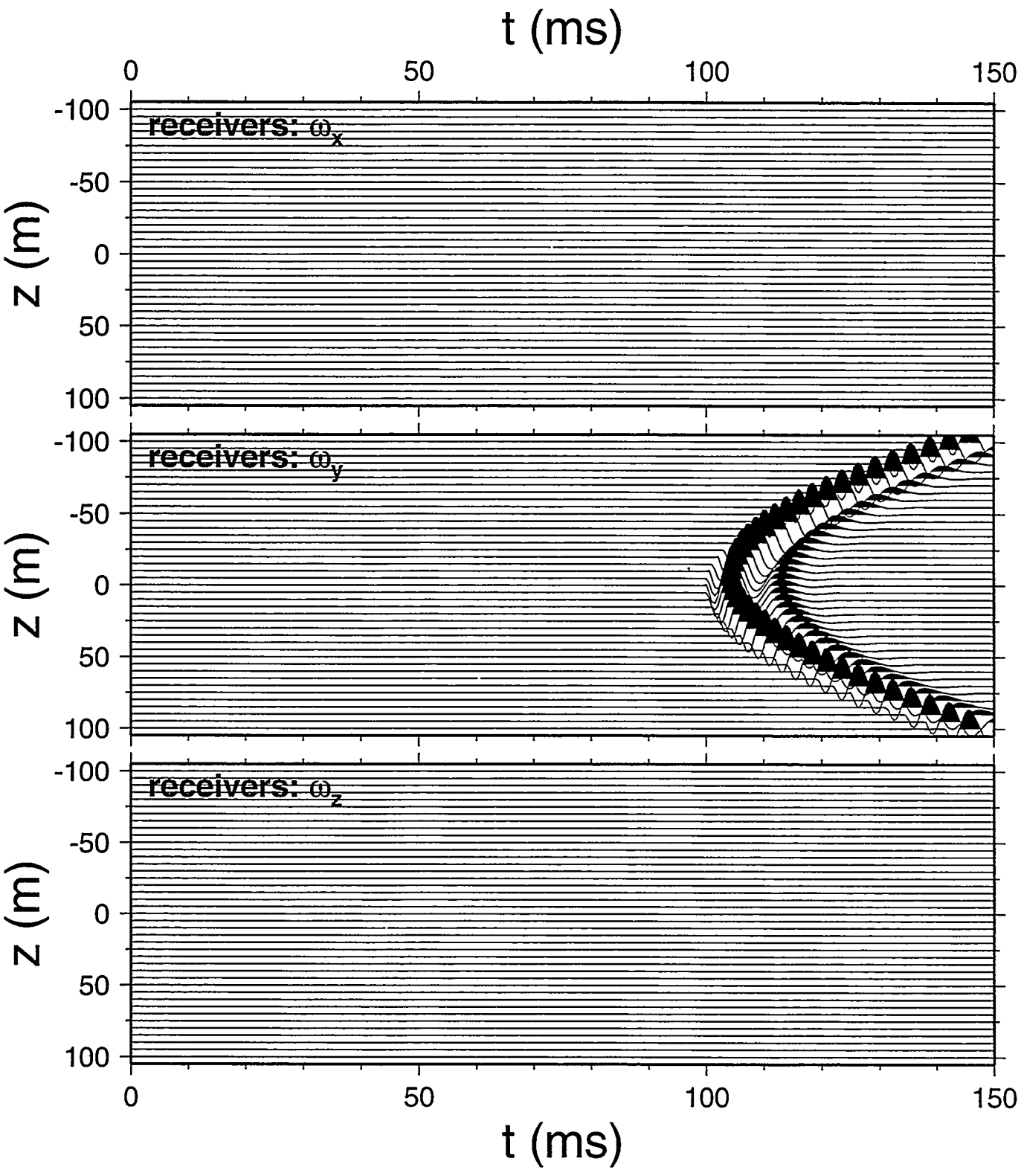

Figure 20 **Source: ty torque**

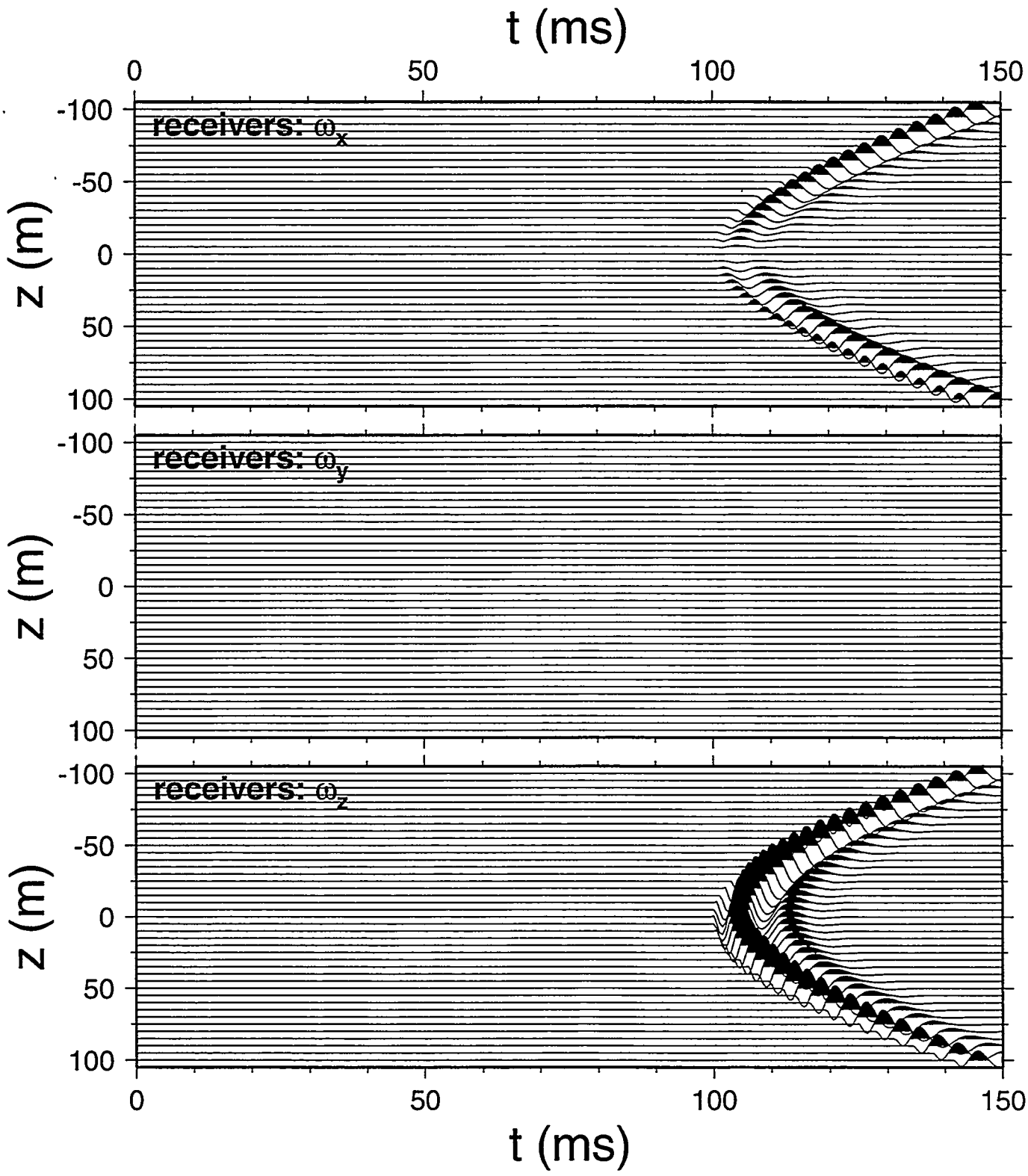

Figure 21 **Source: tz torque**

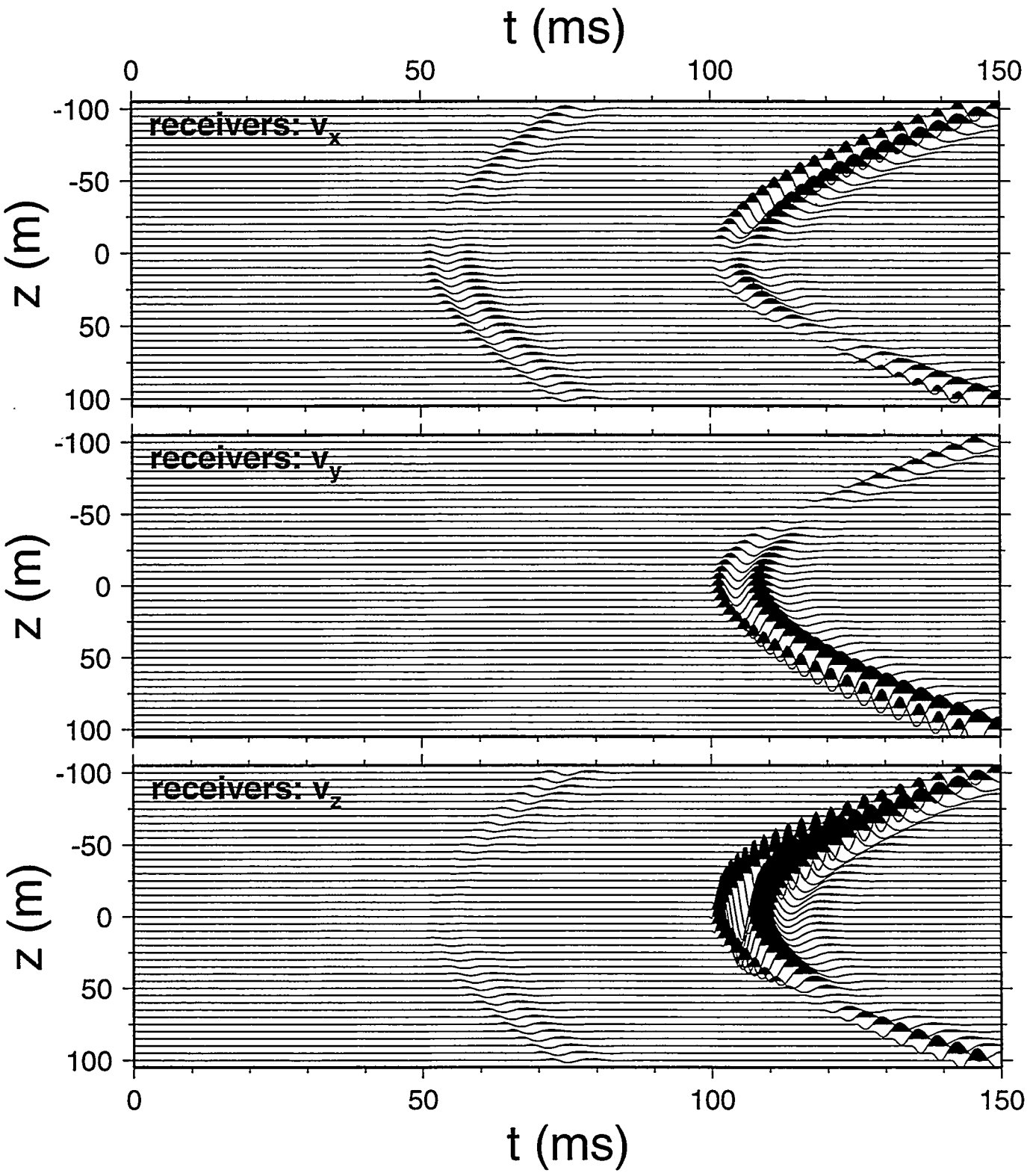

Figure 22

Source: double-couple with no net moment

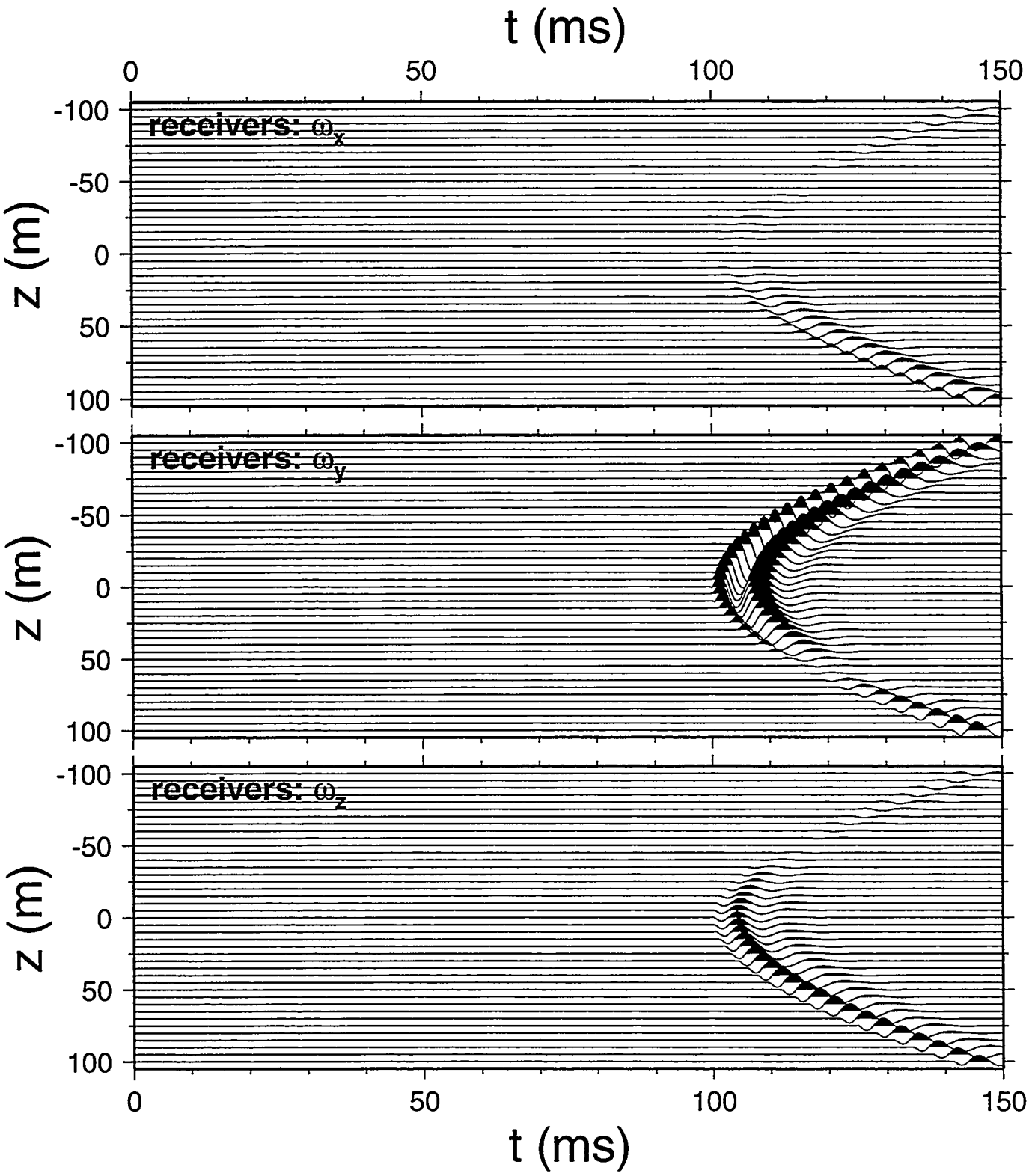

Figure 23

Source: double-couple with no net moment

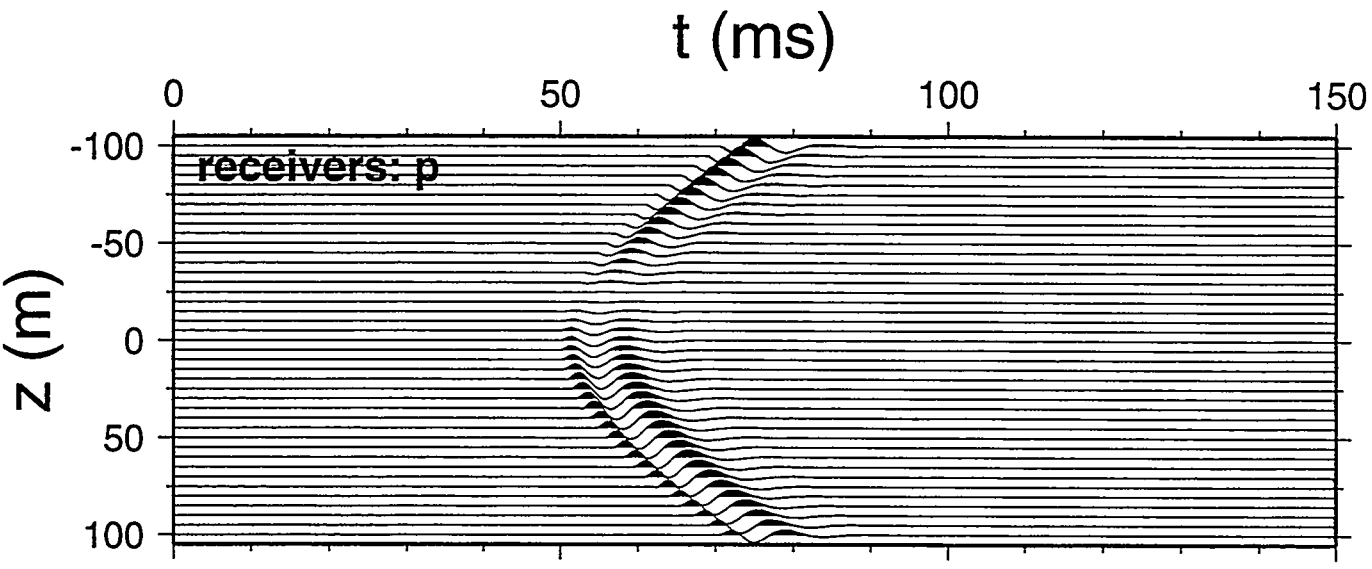

Figure 24

Source: double-couple with no net moment

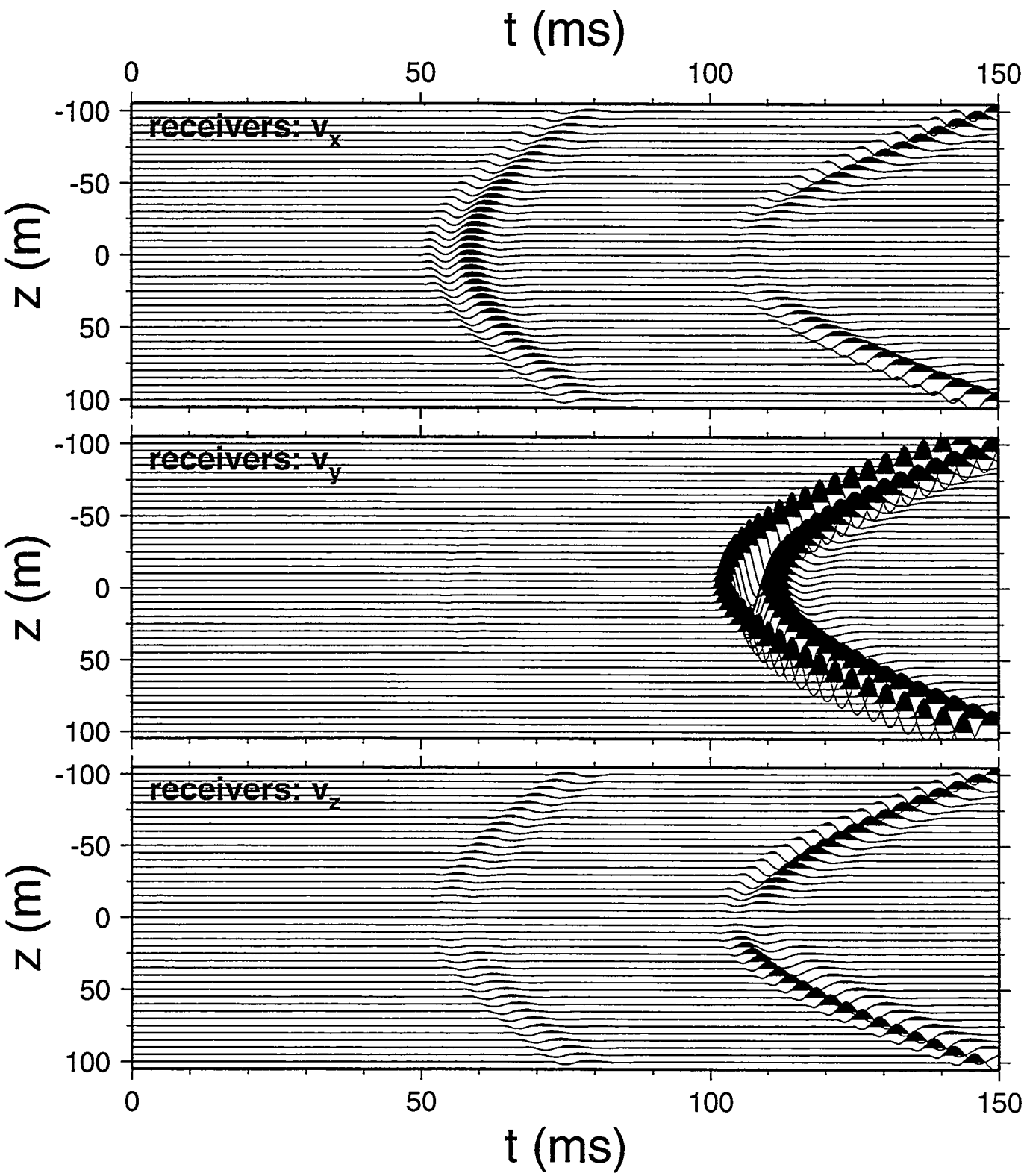

Figure 25

Source: rotating horizontal force

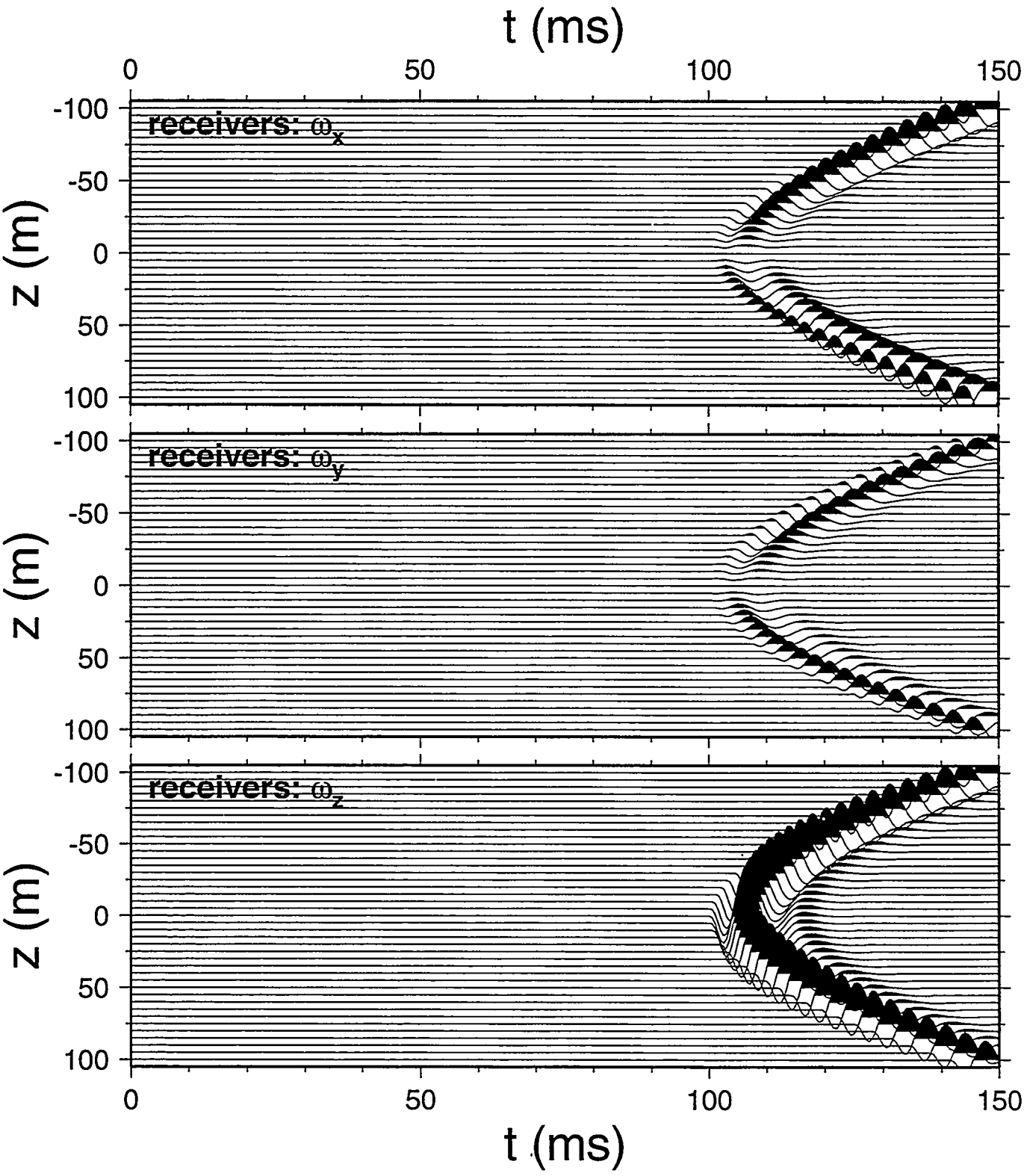

Figure 26

Source: rotating horizontal force

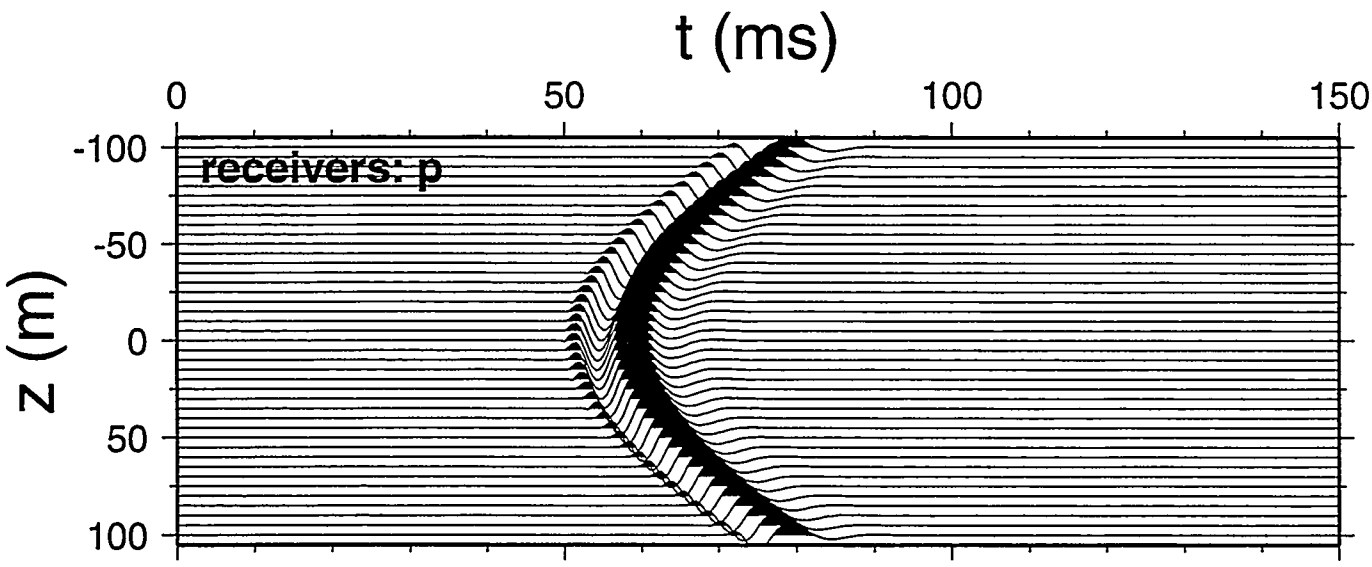

Figure 27

Source: rotating horizontal force

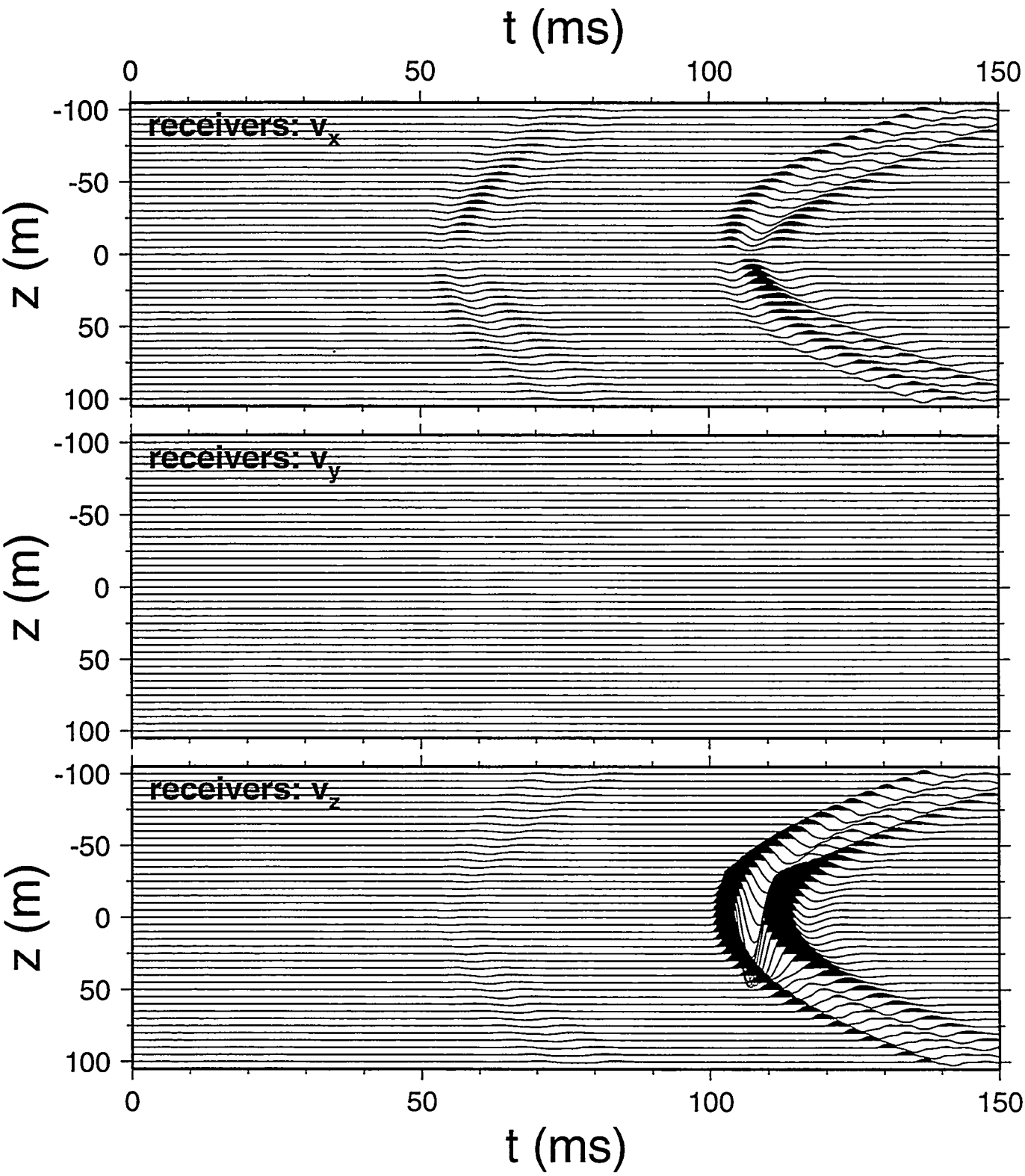

Figure 28

Source: array of 5 f_z forces

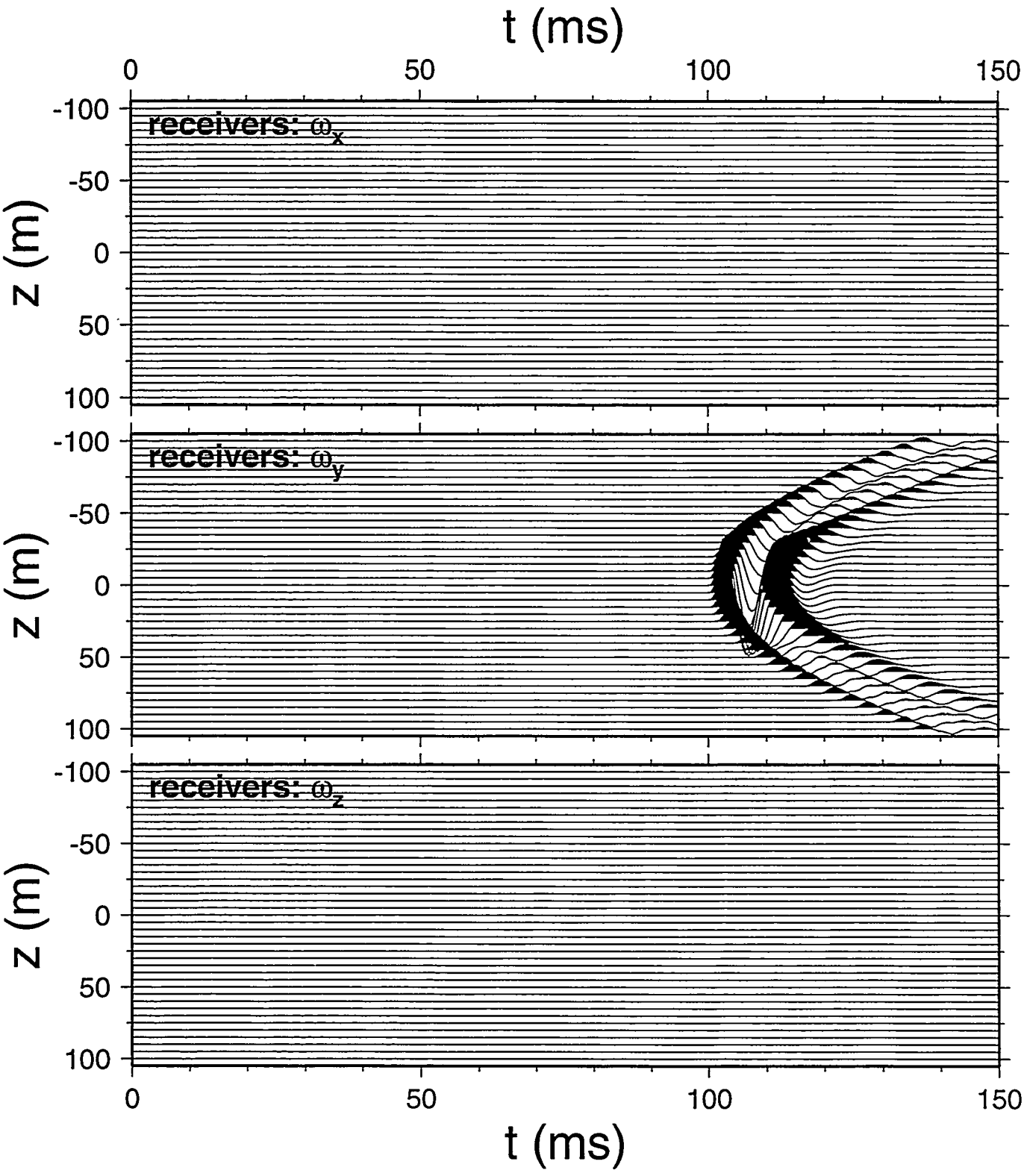

Figure 29

Source: array of 5 f_z forces

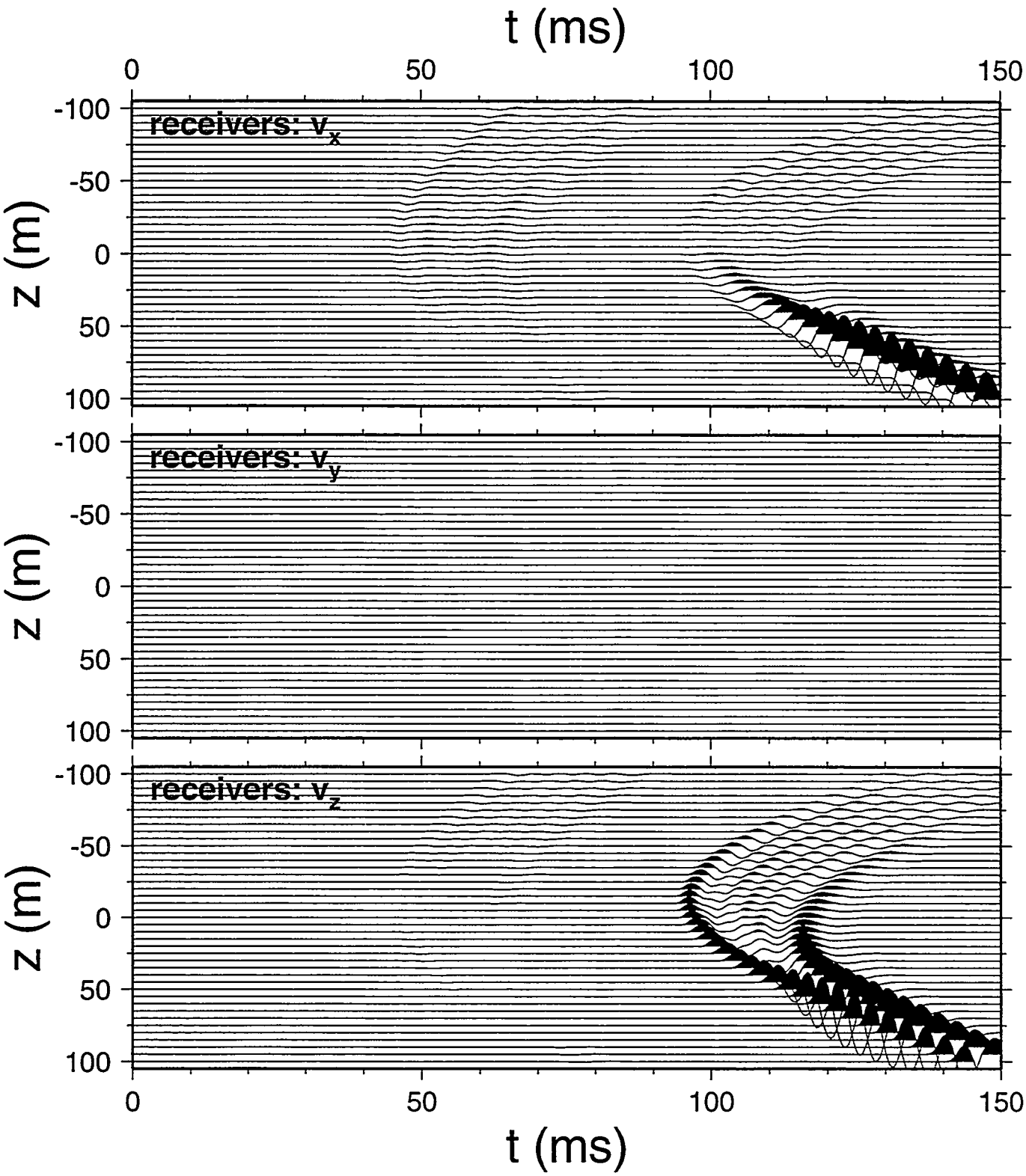

Figure 30

Source: focused array of 5 nonvertical forces

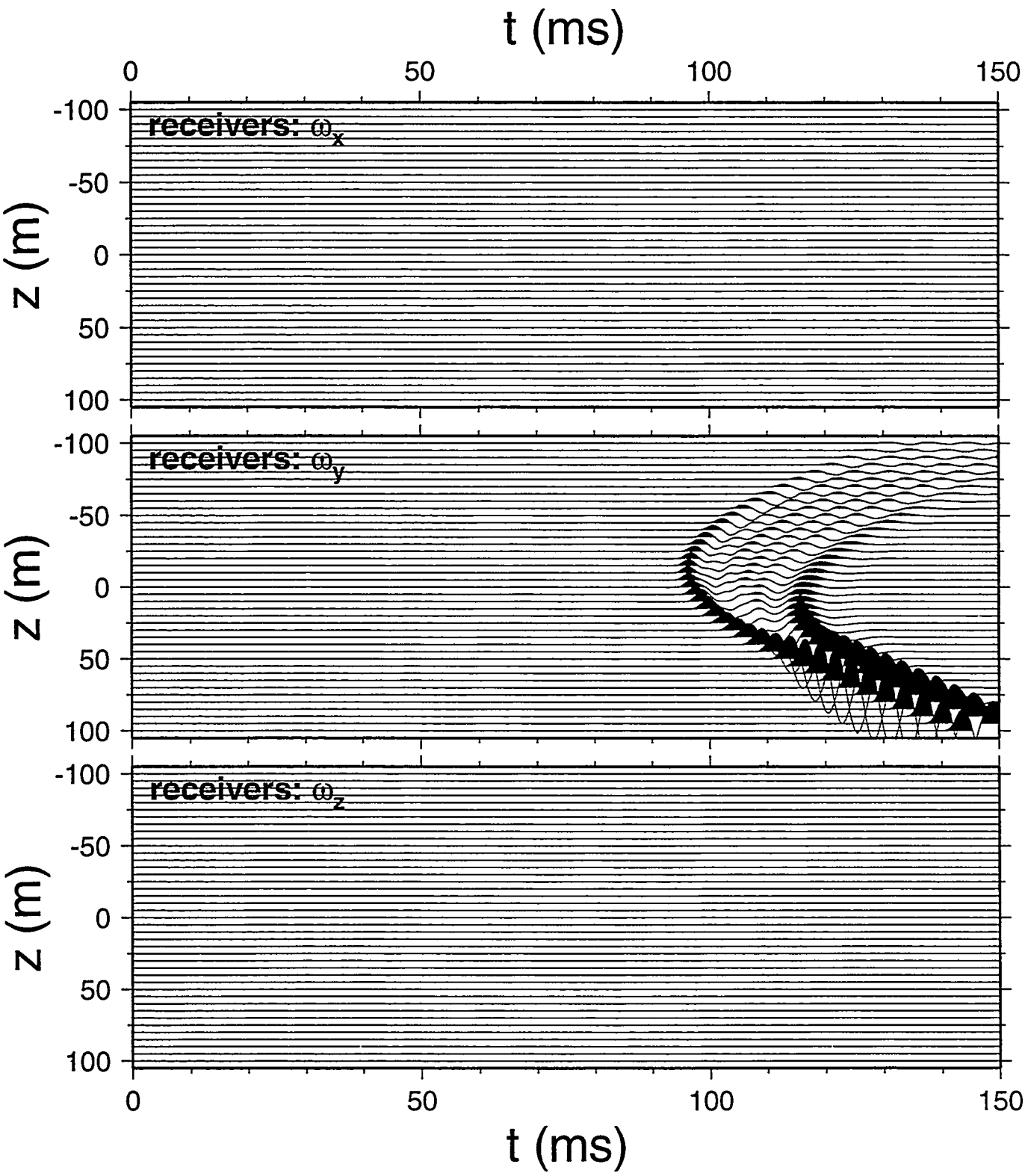

Figure 31

Source: focused array of 5 nonvertical forces

DISTRIBUTION LIST

Sandia National Laboratories Personnel

Organization 1612, Mailstop 1168:
H. Douglas Garbin

Organization 1707, Mailstop 1425:
Marion W. Scott

Organization 5736, Mailstop 0655:
Eric P. Chael
John P. Claassen

Organization 6116, Mailstop 0750:
David F. Aldridge (30 copies)
Sanford Ballard
Lewis C. Bartel
David J. Borns
Thurlow W.H. Caffey
Anthony DiGiovanni
Gregory J. Elbring
Bruce P. Engler
Joanne T. Fredrich
John C. Lorenz
Susan E. Minkoff
Gregory A. Newman
Neill P. Symons
Marianne C. Walck
Norman R. Warpinski
Chester J. Weiss
Christopher J. Young

Organization 6211, Mailstop 1033:
Douglas S. Drumheller

Organization 6533, Mailstop 1138:
Dorthe B. Carr

Organization 9124, Mailstop 0847:
Jeffrey L. Dohner

Organization 9221, Mailstop 1111:
Curtis C. Ober

Organization 9222, Mailstop 1110:
David E. Womble

Organization 15351, Mailstop 0859:
Mark D. Ladd
Gerard E. Sleefe

Technical Library: Organization 9616, Mailstop 0899 (2 copies)

Central Technical Files: Organization 8940-2, Mailstop 9018

Review and Approval Desk: Organization 9612, Mailstop 0612
For DOE/OSTI

Non-Sandia National Laboratories Personnel

Charles C. Burch
Conoco Incorporated
1000 South Pine
PO Box 1267
Ponca City, Oklahoma, 74602-1267

Andrew J. Calvert
Simon Fraser University
Department of Earth Sciences
8888 University Drive
Burnaby, British Columbia, Canada, V5A 1S6

Sen T. Chen
Exxon Mobil Exploration Company
PO Box 4778
Houston, Texas, 77210-4778

Richard T. Coates
Schlumberger-Doll Research
Old Quarry Road
Ridgefield, Connecticut, 06877

V. Dale Cox
Conoco Incorporated
1000 South Pine
PO Box 1267
Ponca City, Oklahoma, 74602-1267

Michael Fehler
Los Alamos National Laboratory
Mailstop D443
Los Alamos, New Mexico, 87545

Brian N. Fuller
Paulsson Geophysical Services Incorporated
8457 East Hinsdale Drive
Englewood, Colorado, 80112

Thomas L. Geers
University of Colorado
Department of Mechanical Engineering
Boulder, Colorado, 80309-0427

Richard L. Gibson
Texas A&M University
Department of Geology and Geophysics
College Station, Texas, 77843-3115

Roland Gritto
Lawrence Berkeley National Laboratory
1 Cyclotron Road
Building 90, Mailstop 1116
Berkeley, California, 94720

Jerry M. Harris
Stanford University
Department of Geophysics
Stanford, California, 94305

Leigh House
Los Alamos National Laboratory
Earth and Environmental Sciences Division
Mailstop D-443
Los Alamos, New Mexico, 87545

G. Michael Hoversten
Lawrence Berkeley National Laboratory
1 Cyclotron Road
Building 90, Mailstop 1116
Berkeley, California, 94720

Brian Hornby
Arco Exploration and Production Technology
2300 West Plano Parkway
Plano, Texas, 75075-8499

John M. Hufford
Phillips Petroleum Incorporated
530H Plaza Office Building
Bartlesville, Oklahoma, 74004

Phillip Inderweisen
Texaco Exploration and Production Technology
3901 Briarpark
Houston, Texas, 77042

Lane R. Johnson
University of California, Berkeley
Department of Geology and Geophysics
Berkeley, California, 94720

Robert T. Langan
Chevron Corporation
935 Gravier Street, Room 1661
New Orleans, Louiisiana, 70112

Ernest L. Majer
Lawrence Berkeley National Laboratory
1 Cyclotron Road
Building 90, Mailstop 1116
Berkeley, California, 94720

Gary F. Margrave
University of Calgary
Department of Geology and Geophysics
Calgary, Alberta, Canada, T2N 1N4

Keith L. McLaughlin
Science Applications International Corporation
1300 North 17th Street, Suite 1450
Arlington, Virginia, 22209

Mark A. Meadows
4th Wave Imaging
850 Glenneyre Street
Laguna Beach, California, 92651

Bjorn N.P. Paulsson
Paulsson Geophysical Services Incorporated
647 South Palm Street, Unit G
La Habra, California, 90631-5794

James W. Rector, III
University of California, Berkeley
Department of Materials Science and Mechanical Engineering
557 Evans Hall
Berkeley, California, 94720

Gerard T. Schuster
University of Utah
Department of Geology and Geophysics
Salt Lake City, Utah, 84112

M. Nafi Toksoz
Massachusetts Institute of Technology
Earth Resources Laboratory
42 Carleton Street
Cambridge, Massachusetts, 02142

Roger Turpening
Massachusetts Institute of Technology
Earth Resources Laboratory
42 Carleton Street
Cambridge, Massachusetts, 02142

David M. Weinberg
Idaho National Engineering and Environmental Laboratory
PO Box 1625
Idaho Falls, Idaho, 83425-2110

Nicholas B. Woodward
U.S. Department of Energy
Geosciences Research Program
19901 Germantown Road
Germantown, Maryland, 20874-1290